Received 11 June 2020; accepted 29 June 2020. Date of publication 7 July 2020; date of current version 24 July 2020.

Digital Object Identifier 10.1109/OJCOMS.2020.3007171

A Wideband Spectrum Sensing Approach for Cognitive Radios Based on Cepstral Analysis

AZZA MOAWAD [1,2] (Member, IEEE), KOFFI-CLÉMENT YAO [3] (Member, IEEE), ALI MANSOUR [4] (Senior Member, IEEE), AND ROLAND GAUTIER [5] (Member, IEEE)

[1] Electronics and Communications Engineering, Arab Academy for Science and Technology, Cairo 11769, Egypt

[2] Lab-STICC, University of Western Brittany, 29238 Brest, France

[3] Security, Intelligence and Integrity of Information Team, Laboratory for Science and Technologies of Information, Communication and Knowledge (Lab-STICC-UMR CNRS 6285), Intelligence and Integrity of Information, University of Western Brittany, 29200 Brest, France

[4] Ecole Nationale Supérieure de Techniques Avancés Bretagne (ENSTA-Bretagne), Lab-STICC, UMR 6285, ENSTA Bretagne, 29806 Brest, France

[5] Signal Processing Team, Lab-STICC-UMR CNRS 6285, University of Western Brittany, 29200 Brest, France

CORRESPONDING AUTHOR: A. MOAWAD (e-mail: azza.moawad@univ-brest.fr)

ABSTRACT Multiband spectrum access plays an essential role in cognitive radio systems so as to increase the network's throughput through wideband spectrum sensing. It includes identifying the number of subbands comprising a wide spectrum by edge detection, and also examining their occupancy through primary user detection techniques. Despite the offered accuracy of the wavelet-based approaches, their complexity becomes a drawback. Remarkably, the features revealing property of cepstral analysis and its implementation simplicity make it a suitable candidate for signal detection. Motivated by these reasons, this paper presents a wideband spectrum sensing approach based on cepstral analysis. First, we propose the differential log spectral density algorithm for the edge detection phase in order to detect the spectral boundaries within the wideband of interest. Also, we present a mathematical framework of the proposed algorithm and an expression for the detection threshold of the proposed detector is derived. The simulation results have showed a superior performance of the edge detection algorithm to different wavelet-based techniques at low-to-medium noise power. Used in conjunction with denoising, the proposed edge detector shows good detection results at low signal-to-noise ratio. For the primary user detection phase, we introduce the improved passband autocepstrum detector to tackle the misdetection problem of noise-like signals and it outperforms different state-of-the-art techniques. Finally, the uncertainty problem of the subbands center frequencies is addressed and the baseband autocepstrum detector is introduced as a potential solution to improve signal detection in frequency selective fading.

INDEX TERMS Baseband autocepstrum detector, cognitive radio, differential log spectral density, wideband spectrum sensing.

NOMENCLATURE

5G	Fifth Generation mobile system
6G	Sixth Generation mobile system
ACE	AutoCorrelation Estimator
AWGN	Additive White Gaussian Noise
BB-ACD	BaseBand-AutoCesptrum Detector
BED	Broadened Energy Detection
CA	Cesptral Analysis
CFD	Cyclostationary Feature Detection
CR	Cognitive Radio
CS	Compressive Sensing
CTF	Circular Topological Filter
DLSD	Differential Log Spectral Density
DSA	Dynamic Spectrum Access
DWT	Discrete Wavelet Transform
ED	Energy Detection
FCC	Federal Communication Commission
FT	Fourier Transform

HF	Hilbert Filtering
MBSA	Multiband Spectrum Access
MFD	Matched Filter Detection
MM	Majorization-Minimization algorithm
NBSS	NarrowBand Spectrum Sensing
PB-ACD	PassBand-AutoCepstrum Detector
PSD	Power Spectral Density
PU	Primary User
SBSA	Single-Band Spectrum Access
SLD	Square-Law Device
SNR	Signal-to-Noise Ratio
SS	Spread Spectrum
SU	Secondary User
TVD	Total Variation Denoising
WBD	Wavelet-Based Detection
WBSS	Wideband Spectrum Sensing
WED	Weighted Energy Detection
WT	Wavelet Transform
WTMM	Wavelet Transform Modulus Maxima
WTMP	Wavelet Transform Multiscale Product
WTMS	Wavelet Transform Multiscale Sum.

I. INTRODUCTION

COGNITIVE Radio (CR) technology thrusts itself as a suitable candidate to solve the problem of scarce radio resources. The evolution of communication technologies aims to fulfill the needs for higher data rates and the increased number of users [1]. Such technology, which is endowed with spectrum awareness, can be integrated with the next cellular wireless standards. For instance, one of the primary goals of the 5G technology is to bring and interconnect wireless and wired systems with a large variety of services, which requires the cooperation of the CR technology. However, the practical deployment of 5G-CR based system poses challenges in the network infrastructure and limits the integration between both technologies [2].

Despite the fact that the commercial 5G networks are currently hardly operational in some countries, this has not stopped engineers to think towards 6G technology that is concerned with adaptivity, cognition, and resiliency of communication. This makes the CR approaches and concepts are good candidates to be realized in 6G [3]. For this purpose, the first global summit on the 6G wireless standards was held at the beginning of 2019 to discuss some academic speculations about the possible potentials of 6G technology. Further, the Federal Communication Commission (FCC) has announced the opening of the terahertz wave spectrum, ranging from 95 GHz to 3 Terahertz (THz), for experiments on the next standards, as well as a full of a 21.5 GHz spectrum for testing of unlicensed devices [4]. Therefore, this wide spectrum entails seeking more spectral opportunities. This can be possible by employing a suitable Wideband Spectrum Sensing (WBSS) technique and hence allows for a potential 6G-CR based systems. Apparently, the research concerns of multiband spectrum access are compatible with the evolution of future communication technologies.

In CR, Dynamic Spectrum Access (DSA) techniques permit the spectrum sharing of unlicensed users [5]. This is to allow a Secondary User (SU) (i.e., unlicensed user) to access different frequency bands in a wide defined spectrum. Generally, there are two types of DSA techniques: the Single-Band Spectrum Access (SBSA), and the Multiband Spectrum Access (MBSA). The former type implies that a SU can access a single narrow frequency band after checking its suitability for a specific spectrum sharing model, whereas the MBSA type refers to accessing a large spectrum that consists of a group of narrow bands. The importance of applying MBSA, despite the complexity of the system, lies in its valuable advantages. Indeed, the handoff frequency with different frequency bands, as well as the interruption of the transmitted SU data due to the sudden resumed activities of Primary Users (PU) (i.e., licensed users) can be reduced. Needless to say, the possibility of accessing multiple narrow frequency bands can enhance the throughput of a CR network and this can be achieved by employing the appropriate WBSS technique.

The process of sensing a wide radio spectrum is performed through two phases, namely: the edge detection phase, and the PU detection phase. Through the edge detection phase, the wide spectrum of interest is analyzed to identify the spectral boundaries, which are characterized by irregularities appearing in the spectrum. For instance, The Wavelet-Based Detection (WBD) approaches employ Wavelet Transform (WT) as a powerful mathematical tool for singularities detection [6]. These singularities, which represent irregular signal structures, define the subband edges (i.e., boundaries). As for the PU detection phase, one of the conventional NarrowBand Spectrum Sensing (NBSS) techniques can be utilized, such as Energy Detection (ED), Matched-Filter Detection (MFD), Cyclostationary feature detection (CFD), and Compressive Sensing (CS) [7]. In general, there are two main methods to apply NBSS: Sequentially, or through parallel sensing. In the sequential sensing method, a narrowband detector senses multiple bands in a serial manner. The major disadvantage of employing sequential sensing is the slow processing time, and also the requirement of re-tuning the used filters and oscillators. While the theme of the parallel sensing method assures a better processing time, the increased complexity of the CR receiver architecture becomes a drawback. This increased complexity is due to the integrated multiple narrowband detectors at the CR receiver.

Since possible errors in the edge detection result consequently affect the performance of the PU detection phase, the crucial challenge in applying the WBSS techniques is the devised edge detection algorithm. In other words, false alarms can be generated due to the presence of spurious edges caused by noisy spectral variations. Moreover, errors in estimating the location of an exact spectral boundary may lead to the misdetection problem. Thus, the promising accuracy of the chosen edge detection approach is vital to assure the overall efficiency of the WBSS process. Clearly, further advancements in wideband sensing are required to provide

high detection robustness against noisy spectral variations with offered low complexity. Therefore, we should highlight the trade-off between the detection accuracy, and the computational burden or the offered hardware complexity. For example, even though the wavelet-based detector provides a reliable detection accuracy in an Additive White Gaussian Noise (AWGN) channel on the one hand, but on the other hand, its hardware and computational complexities are significant. This is because a wavelet-based detector is implemented as a bank of multiresolution filters; So for better detection results, the signal analysis is carried out through all dyadic scales which increases the computational cost.

Moreover, the CS exploits the signal sparsity in the frequency domain knowing that a scarce or underutilized spectrum is sparse. This sparsity invokes a few numbers of measurements to be used, hence a performance degradation is expected due to the reduced Signal-to-Noise Ratio (SNR) despite the hardware simplicity of the CS detector. Motivated by these insights, in this work, we present a novel WBSS technique that is based on the Cepstral Analysis (CA) in the context of CR. We introduce a novel edge detection algorithm based on calculating the Differential Log-Spectral Density (DLSD) of the received wideband signal. This is to identify the spectral boundaries and characterize the number of occupied subbands. In order not to confuse the readers, evaluating the DLSD is slightly different than the conventional differential cepstrum. For a given signal, the DLSD evaluates the derivative of the natural logarithm of the signal's Power Spectral Density (PSD), whereas the differential cepstrum calculates the derivative of a signal's Fourier Transform (FT). A mathematical framework of the proposed edge detection algorithm is analytically illustrated to show the effect of the noisy spectral fluctuations on the resultant spectral boundaries. The proposed algorithm is compared to different wavelet-based edge detection algorithms at different noise power levels to validate its efficacy.

In the literature, the CA has a strong impact on several applications comprising audio and speech processing, as well as mechanical systems. It is also employed in the fields of signal classification or feature detection [8]. Thus, the CA approach is used to identify certain features hidden in a signal that can be revealed in the cepstral domain.

The concept of cepstrum was firstly introduced by Bogert, Healy, and Tukey to analyze time series in the logarithmic frequency domain [9]. Their investigations revealed that the logarithmic spectrum of a signal containing echoes has an additive component reflecting the size and the delay of the echo. Moreover, they introduced new terminologies such as: the *cepstrum* and also *quefrency*. In the literature, the cepstrum is generally defined as the IFT of the logarithmic magnitude spectrum of a signal. Cepstral analysis has been widely used in audio and image processing for its ability to reveal hidden features about signals. According to the variants of the CA approach, a certain CA variant is chosen to fit a specific application. That is why a researcher must be aware of the problem under analysis, and whether employing the CA approach will unleash significant details about the signal in the logarithmic domain. For example, the cepstrum of a pure sinusoidal signal does not show significant peaks, however, an echoed version added to it could show such significance.

By completing the edge detection phase, we eventually obtain the required information about the spectral boundaries of the sensed wide spectrum. Afterward, we proceed to identify the presence of possible PUs in the sensed frequency bands. For example, the authors in [10], and [11] developed a spectrum detector based on a Hidden Markov Model (HMM) with an energy detector front end for offline and online spectrum sensing of narrowband channels. Also, the ED technique can be considered for NBSS since it is a versatile technique that does not require prior information about the PU signal. However, its susceptibility to noise variations results in a poor performance in low SNR environments [12]. While taking advantage of its implementation simplicity, improvements have been made on the ED to gain an acceptable performance in a low SNR scenario [13].

Employing the ED technique for detecting a PU signal assumes that the frequency band of interest is exactly defined and recognized by its spectral boundaries. However, in WBSS, the performance of ED deteriorates. Since the PSD level within a certain subband is evaluated by the integration of the PSD over certain frequency bands, it should take into account the PSD level within the estimated frequency boundaries which are subjected to possible errors. Also, in the case of practical blunt spectrum shapes, the PSD leakage related to the PU signal outside the spectral boundaries will not be considered in the energy calculation [14]. Thus, this may cause the misdetection of a PU. To overcome these drawbacks, the Broadened ED (BED) and the Weighted ED (WED) are suggested in [14]. However, the increased resulting complexity is pushing ED to lose its simplicity property amongst different semi-blind NBSS techniques.

As an alternative approach to the conventional energy detector, we propose two PU detection techniques that are based on evaluating the appropriate signal cepstrum for detecting noise-like signals for the case of the SBSA. It is worth mentioning that in [15] we proposed the PassBand AutoCepstrum Detector (PB-ACD) that analyzes the received signal in its passband version. Through the PB-ACD, the detection process merely depends on identifying a significant peak in the cepstral domain at the reciprocal of the center frequency of the target spectral band. However, in a low SNR environment (e.g., -15 dB) in which high noisy fluctuations are experienced, identifying this major peak will be a difficult task. For this purpose, we introduce an improved version of the PB-ACD technique by providing a smoothing process. We formulate a novel signal smoothing technique that involves the use of the Total Variation Denoising (TVD) approach through the Majorization-Minimization algorithm (MM).

We start by evaluating the fluctuations of the AutoCorrelation Estimators (ACEs) of the received noise-like signal (i.e., spread spectrum signal) to which we apply the TVD-MM algorithm, and then estimating the smoothed spectrum before applying the PB-ACD approach. Since we assume working in a noncooperative detection environment and knowing that most of the denoising techniques depend on some knowledge provided of the received signal, noise statistics, and channel information, we apply the TVD-MM algorithm in semi-blind theme without prior knowledge of the nature of the noise-like signal. Precisely, we utilize the fact that the fluctuations of the autocorrelation estimators of the received SS signal and that of the AWGN are distinguishable [16], the TVD-MM algorithm is applied on the ACE of the received CR signal utilizing this discriminating feature. The purpose of applying the smoothing process is to reduce possible false alarms.

Although the PB-ACD technique has shown its efficacy in detecting a Direct Sequence-Spread Spectrum (DS-SS) signal in [15], with an exact knowledge of the subbands center frequencies, its performance deteriorates when applied in the MBSA scenario due to the potential errors in estimating the subbands center frequencies. These errors may result in the misdetection and false-alarm problems. As a solution, we introduce the BaseBand AutoCepstrum Detector (BB-ACD) that exploits the periodicity feature that can be revealed of the baseband digital signals in the cepstral domain. Accordingly, we propose a non-coherent detection of the received signal via a Circular Topological Filter (CTF), which consists of Hilbert Filtering (HF) and a Square-Law Device (SLD). This is to extract the baseband version of a signal before evaluating the power cepstrum of the received signal so that the detection process does not depend on the exact knowledge of the center frequency of a specific subband.

Specifically, the main contributions of the proposed wideband spectrum sensing approach through the CA can be listed as follows:

1) For the edge detection phase, we propose the DLSD algorithm to identify the spectral boundaries of the subbands comprising the target wideband spectrum.
2) A mathematical framework of the DLSD approach is illustrated.
3) An analytical expression of the detection threshold characterizing the proposed DLSD detector is derived.
4) The performance of the PB-ACD technique is tested in Rayleigh fading channel and compared with ED for detecting OFDM PU signals.
5) The improved PB-ACD technique is presented to detect noise-like PU signals that may be miss-detected in noisy channels. The proposed technique is provided by the employment of a signal smoothing process which includes applying the TVD-MM algorithm to the fluctuations of the ACEs of the received signal to reduce the unwanted spectral fluctuations.
6) The BB-ACD technique is formulated for the PU detection phase in wideband spectrum sensing in order to address the uncertainty problem of the subbands center frequencies. The proposed technique exploits the inherited periodicity of the baseband digitally modulated signals in the cepstral domain. A mathematical analysis of the detection threshold is developed. Simulations have shown that the BB-ACD technique outperformed the PB-ACD technique when the uncertainty problem of the subband center frequencies is encountered.
7) We also extend our proposed BB-ACD technique to consider mobile targets such as OFDM PU signals in frequency selective fading channels with Doppler frequency shifts and it proved its detection efficacy.

The rest of the paper is organized as follows. Section II gives a brief state-of-the-art on the applications of CA in CR and also summarizes the advantages and critics of the wavelet-based edge detection techniques. Section III states the mathematical foundation of the problem under investigation and describes the overall proposed system architecture. The proposed edge detection and the CA-based PU detection techniques are introduced in Section IV, with the mathematical analysis of both techniques. In Section V, the numerical results are illustrated, and the conclusions are drawn in Section VI.

II. STATE-OF-THE-ART

The process of wideband spectrum sensing starts with detecting the edges of the spectral boundaries. Many pieces of research have presented the process of edge detection as a peak detection problem. The notion of a peak depends on the function representing the required set of peaks in a signal. A peak function is one that characterizes a peak detector. It captures the spikiness of a significant feature in a signal, or generally, in a given time-series. Generally, there are some standard approaches to detect peaks, such as:

i Fitting a smoothed time series to a known function (e.g., wavelet analysis).
ii Matching a known peak shape to a given time series.
iii Detection of zero-crossings in the differences between specific points and its neighbors (e.g., Hilbert Filtering) [17].

Amongst many peak detection approaches, the wavelet analysis approach is significant in determining sharp variations that appeared in a signal. So, in this section, we present a brief overview of the WBD techniques. Further, we illustrate the applications of CA in CR and the importance of applying CA in the WBSS problem as compared to the WBD techniques.

A. WAVELET TRANSFORM FOR EDGE DETECTION

Wavelet analysis is considered as an efficient mathematical tool to describe the irregular structure in a signal by defining its singularities. Based on this concept, it has been

adopted to identify the boundaries of non-overlapping subbands in a wide spectrum to classify them into white, gray, or black spectral holes. In [18], Tian and Giannakis introduced the use of WT Modulus Maxima (WTMM) approach to allocate wideband edges and hence simultaneously identify all piece-wise flat frequency bands. One major limitation of this approach is its sensitivity to noisy fluctuations. Even by thresholding, all spurious components cannot be eliminated. Further, the authors suggested the use of WT Multiscale Product (WTMP), to enhance the multiscale modulus coefficients while suppressing noise. However, this results in miss-detecting an exact edge that is heavily corrupted with noise. On the other hand, WTMP exploits the correlation provided to improve the detection performance. The disadvantages of this approach are the loss of signal details, and losing the property of the multiresolutional analysis to distinguish between narrowband and wideband signals. To reduce this effect, the authors of [18] suggested the analysis of small and large scales separately. As an alternative approach, WT Multiscale Sum (WTMS) was introduced in [19] for information preservation as well as avoiding attenuation that possibly occurs because of multiplication operations.

Despite the offered advantage of the WTMS over the WTMP, the dramatic increase of the scales throughout the analysis causes edges localization loss. A solution to this problem has been addressed in [20] by employing a non-orthogonal class of wavelet functions such as the Gaussian wavelet function. Moreover, Jindal *et al.* in [21] has tested the work of Tian and Giannakis in multipath fading channels, and they found that a good performance is achievable in moderate fading, but it is dropped significantly in deep fading channels. In [22], the authors suggested applying a logarithmic scaling preceded by thresholding in order to enhance the small modulus maxima values at the exact edges. However, the computation burden becomes a consequence of applying their proposed technique. Also, this enhancement affects negatively the spurious edges by magnifying them. This increases false alarms at high noise variance. In this sense, Discrete WT (DWT) based algorithm is suggested in [22] to alleviate this problem. The DWT algorithm can perform edge detection and denoising simultaneously providing reliable performance in high SNR scenarios. In the case of low SNR scenarios, a moving averaging filtering strategy is adopted. As a result, better performance is achieved at lower scales, thus the computation time is reduced on the expenses of the increased hardware complexity. Further details concerning challenges, advantages, and disadvantages of multiband spectrum access techniques in CR can be found in [23].

B. APPLICATION OF CEPSTRAL ANALYSIS IN COGNITIVE RADIO

Cepstral Analysis (CA) is a logarithmic based approach for detecting signal features. Analyzing a given signal in the cepstral domain has gained much interest in different fields of signal processing. Transforming the signal of interest from time to frequency domains and getting the inverse Fourier transform of its natural logarithm results in representing the signal in neither time nor frequency domain. So in order to forestall the conceptual confusion of operating on the frequency side that is customary on the time side, Bogert *et al.* chose to refer to such domain as the quefrency domain [9]. In literature, there are several methods to employ the cepstrum of a signal. Table 1 gives a summary of famous cepstral variants. First of all, let us define the following variables:

- n: The discrete time domain.
- $x(n)$: The analyzed discrete time domain signal.
- k: The discrete frequency variable.
- $X(k)$: The Fourier Transform of $x(n)$.
- $\mathcal{F}\{.\}$, and $\mathcal{F}^{-1}\{.\}$: The Fourier and inverse Fourier transform operators, respectively.
- $\hat{n}$: The discrete quefrency variable, which is a measure of alternative time in the cesptral domain [24], [25].
- $R_x(l)$: The discrete autocorrelation function of the signal $x(n)$ at a time lag of l.
- $X'(k)$: The first derivative of $X(k)$.

As it was previously mentioned, CA has been utilized differently in the field of signal detection. For example, it has been applied for echoes detection in seismic waves [26]. Further, it has been used to estimate the multipath time delay as introduced in [27], or for detecting audio watermarks [28]. In the contexts of spectrum sensing and signal detection in CR, CA approaches have been rarely utilized. For instance, the authors in [29] have employed CA techniques in waveform classification and for detecting OFDM signals and also for estimating their parameters. Moreover, the authors of [30] have introduced a WideBand Temporal Sensing (WBTS) approach based on a cepstral envelope detector. Precisely, the involvement of the cepstrum-based spectrum envelope detector is to adapt to dynamic changes that may occur in the configuration of a PU channel. The rationale of this approach is to use a cepstral feature vector to detect the changes in the spectrum envelope of a PU signal within a given frequency band. Based on the recursive temporal spectrum sensing algorithm proposed in [31], the authors in [30] have proposed the use of cepstral analysis to monitor the change of the PU's configuration instead of the conventional ED front end.

TABLE 1. Variants of the cepstral analysis terms.

Definition	Mathematical Description
Real Cepstrum	$c_R(\hat{n}) = \mathcal{F}^{-1}\{\log\lvert X(k)\rvert\}$
Complex Cepstrum	$c_C(\hat{n}) = \mathcal{F}^{-1}\{\log X(k)\}$
Power Cepstrum	$c_P(\hat{n}) = 4\lvert c_R(\hat{n})\rvert^2$
Differential Cepstrum	$c_D(\hat{n}) = \mathcal{F}^{-1}\left\{\frac{X'(k)}{X(k)}\right\}$
Autocepstrum	$c_A(\hat{n}) = \mathcal{F}^{-1}\{\log\mathcal{F}\{R_x(l)\}\}$

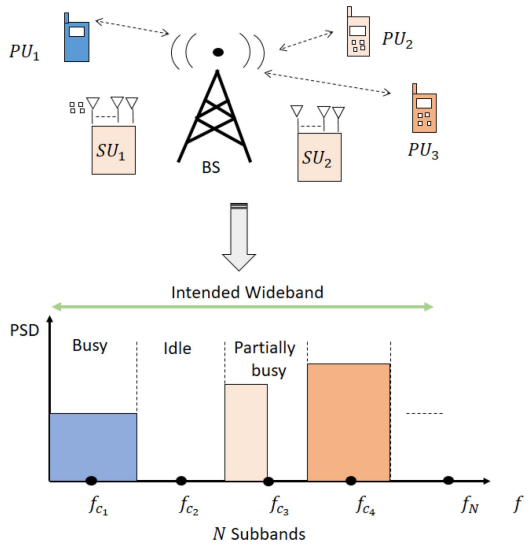

FIGURE 1. Wideband Sensing Problem.

In the WBTS approach, a given frequency band is divided into narrowband channels of equal bandwidths. Every narrowband channel is then sensed individually using an HMM-based approach. The employed HMM model is trained by an observation sequence that consists of average received signal powers. The parameters of the trained HMM model is estimated by the Baum algorithm[1] [31]. According to a modified correlation metric, the adjacent channels are aggregated to form larger channels. After being conducted in a recursive manner, this process eventually results in the identification of a set of PU channels with their HMM estimated parameters. At the same time, a cepstrum-based envelope detector is applied to monitor the transition of the PU channel to a different configuration. The spectrum envelope detector is designed based on the HMM model in which the employed observation vector corresponds to the signal's cepstrum.

Our proposed cepstrum-based WBSS approach differs from the WBTS approach such that it introduces the following:

- Identification of the number of occupied subbands in a target wide spectrum. This is formulated as an edge detection problem and accomplished by developing the DLSD algorithm.
- Detection of noise-like PU signals such as spread spectrum signals. For this purpose, we reviewed our proposed PB-ACD technique in [15] which detects the presence of a DS-SS signal by monitoring a major autocepstral peak. The improved PB-ACD technique is proposed for improving the detection process by providing a smoothing to the fluctuation so the ACEs.
- Detection of noise-like signals under the uncertainty problem of the subbands center frequencies is accomplished by introducing the BB-ACD technique.
- To the best of our knowledge, the proposed WBSS approach is the first to consider the use of the DLSD algorithm for edge detection in CR and also improved PB-ACD technique for detecting noise-like PU signals. Also, exploiting the cepstral features of the baseband signals for PU detection when the uncertainty problem of the subbands center frequencies is relatively novel.

Since our goal is to identify the frequency locations of non-overlapping spectrum bands and detect the presence of spectral holes, the adaptation of CA for WBSS, as opposed to the wavelet-based approach, is motivated by the following insights:

- Using wavelet analysis to the intended spectrum depends on the applied wavelet function, so the accuracy and the performance will also depend on the appropriate choice of the mother wavelet.
- The complexity of the wavelet approach offered, due to the consecutive scaling and shifting operations, affects the sensing time.
- CA decomposes a signal into envelope and excitation components through deconvolution [32]. This filtering signifies the fine details representing fast variations (i.e., high frequency components).
- CA has the property of revealing hidden harmonics and periodic features of analyzed signals.
- CA is lower in the implementation complexity as opposed to wavelet analysis.

III. PROBLEM FORMULATION OF WIDEBAND SPECTRUM SENSING

The main target of employing wideband sensing is to provide more spectral opportunities. It means that the SU must recognize precisely the number of subbands in the wide sensed spectrum before testing the occupancy of each one of them. To design the wideband detector, we should take into account the problem of edge detection and the identification of spectral holes. Further, there are some challenges, facing the design of the wideband detector, that must be clarified. They are summarized as follows:

- The inspected subband may be licensed to certain wireless devices, such that they consume a small portion of the reserved bandwidth, yet the total bandwidth might be considered occupied. In this case, the SU must be aware of the percentage of the spectral occupancy accurately to avoid interfering with the licensed user and to be able to configure properly its transmission to exploit the non-utilized portion. This is illustrated in Fig. 1.
- Subbands are assumed to be non-overlapping and have identical bandwidths; and the occupied channels are uncorrelated, in contrast to systems such as WiLAN and Broadcast TV in which subchannels are correlated.
- The detection of a PU, transmitting a wideband signal in a deep fading channel is challenging because without providing the CR systems with subchannels correlation information, the SU may interfere with the PU when resuming its transmission.

1. The Baum algorithm is a special case of the Expectation-Maximization (EM) algorithm that is used to find the unknown parameters of an HMM.

A. PHASE I: IDENTIFICATION OF SPECTRAL BOUNDARIES

In a cognitive communication network in which heterogeneous wireless devices are supported, a CR user must be able to sense the wireless environment at a specific time and place within a wide spectrum. In particular, the SU must acquire the knowledge of the subchannel edges characterizing the spectral boundaries. Once the boundaries are estimated, we can define their center frequencies, and eventually, the PU occupancy can be examined. In this context, we can formulate the problem statement for edge detection in WBSS as follows:

In order to detect a specific spectral hole in a predefined wide frequency band by a cognitive radio receiver, we need to identify the parameters characterizing the wideband spectral environment which are: the number of subbands N, their corresponding center frequencies $\{f_{c_n}\}_{n=1}^{N-1}$, and the spectral boundaries $\{f_n\}_{n=1}^{N-1}$.

Before representing our proposed solution to this problem, some basic assumptions are drawn:

- The entire wide band under scrutiny is modeled as a train of consecutive frequency subbands, where the power spectral characteristic is analyzed under two conditions:
  - i Piece-wise flat spectrum that exhibits a discontinuous change between adjacent subbands.
  - ii Blunt-shaped spectrum generated by a raised-cosine pulse shaping filter as a practical example.

  These changes are irregularities in the Power Spectral Density (PSD). They carry key information on subband locations.
- The wide spectrum of interest denoted by $\mathcal{B}$ is defined in the frequency range $[f_0, f_N]$ provided that the spectral boundaries f_0 and f_N are known by the CR system.
- The n^{th} subband within $\mathcal{B}$ is defined by $\mathcal{B}_n$ such that: $f \in \mathcal{B}_n : f_{n-1} \leq f < f_n$, and the frequency boundaries of the consecutive bands are denoted by $f_0 \cdots f_N$, where N is the number of frequency bands within $\mathcal{B}$.
- The number of frequency bands is unknown to the CR as well as the frequency boundaries.
- The ambient noise is assumed to be an additive white Gaussian noise, with zero mean and two-sided PSD:

$$S_w(f) = \frac{N_0}{2}, \ \forall f \tag{1}$$

- We consider the case of a slotted medium access in the interweave CR system, by which the SU performs a periodic sensing on segmented time frames.
- The effect of adjacent channel interference is neglected by assuming the n^{th} subband PSD $S_n(f) = 0, \forall f \notin [f_{n-1}, f_n]$.

1) SIGNAL AND CHANNEL MODELS

Let us define the received signal by the CR receiver by:

$$\begin{aligned} r(t) &= s(t) + w(t) \\ &= \sum_{n=1}^{N} s_n(t) + w(t) \end{aligned} \tag{2}$$

where $s(t)$ is the received wideband signal, $w(t)$ is the AWGN signal, and $s_n(t)$ is the signal occupying the $\mathcal{B}_n$, which is given by:

$$s_n(t) = x_n(t) * h_n(t) \tag{3}$$

where $x_n(t)$ is the transmitted signal that is represented by a sequence of a digitally modulated pulses in the n^{th} band. The channel impulse response between the PU and the SU at the n^{th} subband is denoted by h_n, whereas the symbol $*$ denotes the convolution product. In the case of a narrowband channel, we can rewrite (3) as:

$$s_n(t) = a_n \sum_{k=-\infty}^{\infty} b_k \ p(t - kT_s) \ \ \exp(j2\pi f_{c_n} t) \tag{4}$$

where a_n represents the attenuation suffered by the transmitted signal in the n^{th} subband. Also, $\{b_k\}$ are the set of digital symbols, $p(t)$ is the pulse shaping function, and $f_{c_n} = \frac{f_n + f_{n-1}}{2}$ is the subband center frequency. The PSD of the observed signal $r(t)$ at the CR front-end can be written as:

$$S_r(f) = \sum_{n=1}^{N} a_n^2 \ S_x(f) + \ S_w(f), \ f \in [f_0, f_N] \tag{5}$$

where a_n^2 is the PSD level in the n^{th} band due to the channel attenuation, $S_x(f)$ is the PSD of transmitted digital signal, and $S_w(f)$ is the noise PSD.

B. PHASE II: PRIMARY USER DETECTION

Following the edge detection phase, the WBSS problem requires the CR receiver to solve N binary hypothesis testing problems. For an independent subchannel occupancy, the WBSS problem definition can be defined as:

$$\mathrm{r} = \begin{cases} \mathrm{w}: & Under\ {H_o}^n \\ \mathrm{x} + \mathrm{w}: & Under\ {H_1}^n \end{cases} \tag{6}$$

where $\mathrm{r} = [\mathrm{r}_1, \mathrm{r}_2, \mathrm{r}_n, \ldots, \mathrm{r}_N]$ denotes the received signal matrix, w is the noise vector at each subband, and ${H_0}^n, {H_1}^n$ represents the n^{th} null and alternative hypothesis, respectively. As seen from (6), the complexity of the detection problem increases as the number of subchannels increases. The decision rule, represented by the test statistic $T[r_n]$ and the detection threshold ζ_n, can be given by:

$$T[r_n] \underset{{H_0}^n}{\overset{{H_1}^n}{\gtrless}} \zeta_n \tag{7}$$

It is important to indicate that the definition of the test statistic depends on the type of the applied narrowband detector. Also, The formulation of the detection threshold depends on the statistical distribution of the noise in the detector test statistic. In the following sections, we illustrate the proposed approach in both phases.

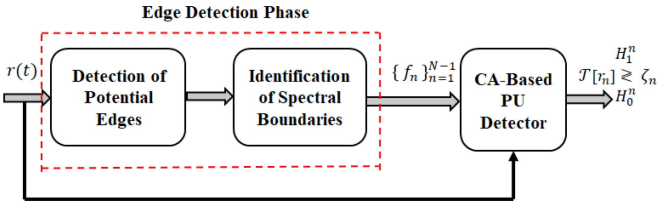

FIGURE 2. The sequence of operations of the proposed WBSS approach.

IV. THE PROPOSED WIDEBAND SPECTRUM SENSING APPROACH

In this work, we develop a complete framework of the WBSS approach based on the CA of the received signal. In our investigation, we seek a reduced system complexity and a reliable detection accuracy in the edge detection and the PU detection phases. The channel estimate at each subband can be provided by the pilot-insertion method after being identified [33].

A. IDENTIFICATION OF SPECTRAL BOUNDARIES BY CEPSTRAL ANALYSIS

First, we introduce the Differential Log Spectral Density technique and mathematically analyze the detection process in the case of high, medium, and low SNR scenarios. The three SNR cases are considered for an example of a wideband spectrum that consists of consecutive subbands, each one has a specific spectral density level. So, based on the average spectral density level, we vary the AWGN power level, denoted by σ_w^2, to consider the three SNR cases. Precisely, for the case of having the SNR < 0 dB (i.e., equivalently the noise power $\sigma_w^2 > 20$ dB), the considered wideband spectrum is analyzed in a low SNR environment. The sequence of operations of the proposed CA-based WBSS approach is shown in Fig. 2.

1) EDGE-DETECTION BY THE DIFFERENTIAL LOG-SPECTRAL DENSITY ALGORITHM

For a compact representation, the PSD of the received signal, defined in (5), can be given by:

$$S_r(f) = S(f) + S_w(f) \tag{8}$$

where $S(f) = \sum_{n=1}^{N} S_n(f)$ denotes the sum of PSDs of the signals occupying the sensed wide spectrum. To apply the DLSD, we perform the following:

1) Evaluate the autocorrelation estimate of the received signal and then, its PSD.
2) Evaluate the first derivative of the autocepstrum of the received signal in the frequency domain.

For convenience, by applying the natural logarithm to (8), we obtain:

$$\begin{aligned} Z_r(f) &= \log S_r(f) \\ &= \log [S_w(f)] + \log\big[\gamma(f) + 1\big] \end{aligned} \tag{9}$$

where $\gamma(f) = \frac{S(f)}{S_w(f)}$ defines the relative PSD variations of the transmitted wideband signal to the noise PSD.

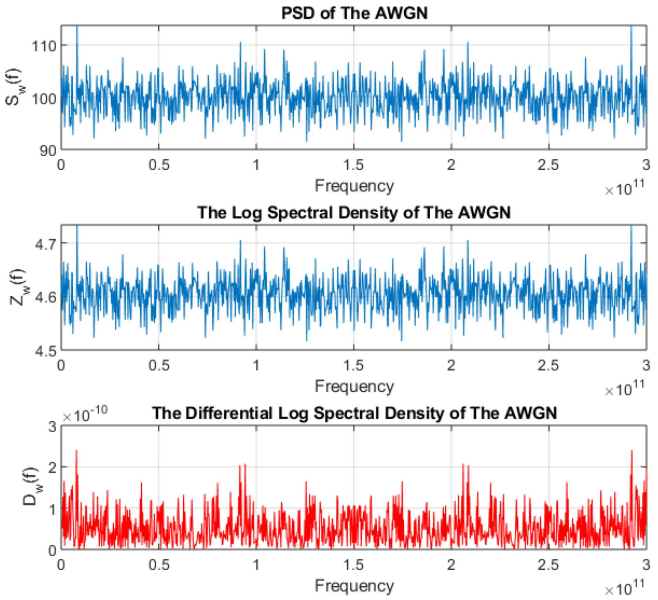

FIGURE 3. Illustration of the effect of applying the DLSD to the AWGN spectrum.

The n^{th} spectral peak identifying the n^{th} subband boundary is located at:

$$f_n = arg\{|D(f)|\}, f_n \in [f_1, f_{N-1}] \tag{10}$$

where $arg(.)$ defines the argument of a function within the round parenthesis, and $D(f) = \frac{d}{df} Z_r(f)$ represents the DLSD function. Accordingly, we need to analyze $Z_r(f)$ in case of a medium-to-high SNR environment as well as a low SNR environment. Since the PSD level of the noise is assumed to be constant, getting its natural logarithm decreases the PSD value. Therefore, the value $Z_w(f) = \log [S_w(f)]$ is much lower than $\log [\gamma(f) + 1]$. By taking the derivative of $Z_r(f)$, we can consider that $D_w(f) = \frac{d}{df} \log [S_w(f)] \approx 0$, then we obtain:

$$D(f) = \frac{d}{df} \log [\gamma(f) + 1] = \frac{1}{1 + \gamma(f)} \frac{d}{df} \gamma(f) \tag{11}$$

substituting equation (8) in (11), we get:

$$D(f) = \frac{1}{S(f) + S_w(f)} \sum_{n=1}^{N} \frac{d}{df} S_n(f) \tag{12}$$

According to (12), and for the case of a medium-to-high SNR, the relative PSD variations is assumed $\gamma(f) >> 1$, then (12) reduces to:

$$D(f) \approx \frac{1}{S(f)} \frac{d}{df} S(f) \tag{13}$$

whereas for the low SNR case, $\gamma(f) << 1$, then we obtain:

$$D(f) \approx \frac{2}{N_0} \frac{d}{df} S(f) \tag{14}$$

To clarify the concept, Fig. 3 shows the low PSD level of the AWGN after applying the DLSD technique and justifies the approximation applied in (11). Fig. 4 gives another example of the wideband spectrum scenario that consists of a group

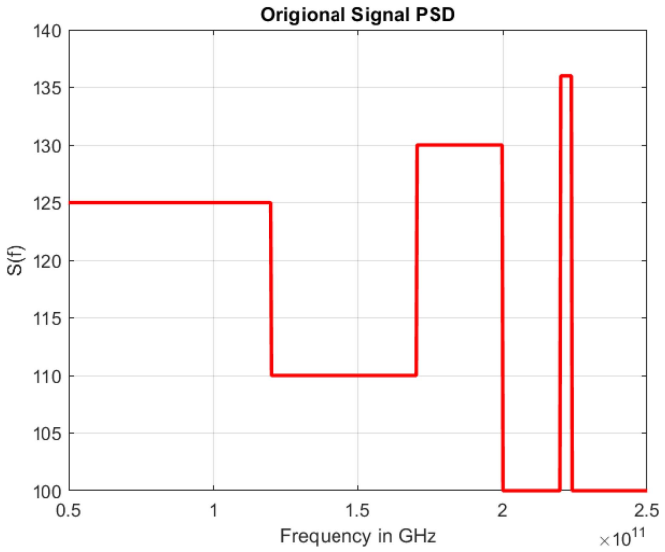

FIGURE 4. An example of a wideband spectrum that consists of consecutive subbands.

TABLE 2. The SNR specifications per subband of an example of a wideband spectrum.

Band Order	Band Range (GHz)	PSD Level (dB/Hz)	High SNR $\sigma_w^2 = 14.7$ (dB)	Medium SNR $\sigma_w^2 = 20$ (dB)	Low SNR $\sigma_w^2 = 24$ (dB)
1	50-120	21	6.3	1	-3
2	120-170	20.4	5.7	0.4	-3.6
3	170-200	21.1	6.4	1.1	-2.9
4	200-220	20	5.3	0	-4
5	220-225	21.3	6.6	1.3	-2.7
6	225-250	20	5.3	0	-4

of consecutive flat piece-wise subbchannels. In that example, the wideband spectrum is ranging from 50 to 250 GHz, such that each subband has a specific spectral density level within its corresponding bandwidth. Also, Table 2 indicates the SNR values for each subband with respect to the noise variance.

The effect of applying the proposed DLSD technique for the case of low, medium, or high noise power with respect to the average PSD level of the consecutive subbands is illustrated in Fig. 5, Fig. 6, and Fig. 7. For the case of low and medium noise variances (precisely, $\sigma_w^2 = 14.7$ dB and $\sigma_w^2 = 20$ dB), the spectral boundaries are clearly distinguishable from the noisy edges. When the noisy spectral variations are high, as shown in Fig. 7, the actual spectral boundaries are hardly being differentiated from the spurious edges and may result in detection errors. To solve the high noisy spectral peaks, we employed the TVD-MM algorithm to reduce the noisy spectral fluctuation before applying the DLSD. Indeed, we notice that if the average SNR < 0 dB ($\sigma_w^2 > 20$ dB), the spectral edges of the subbands can be well identified when the DLSD technique is applied in conjunction to denoising as shown in Fig. 8.

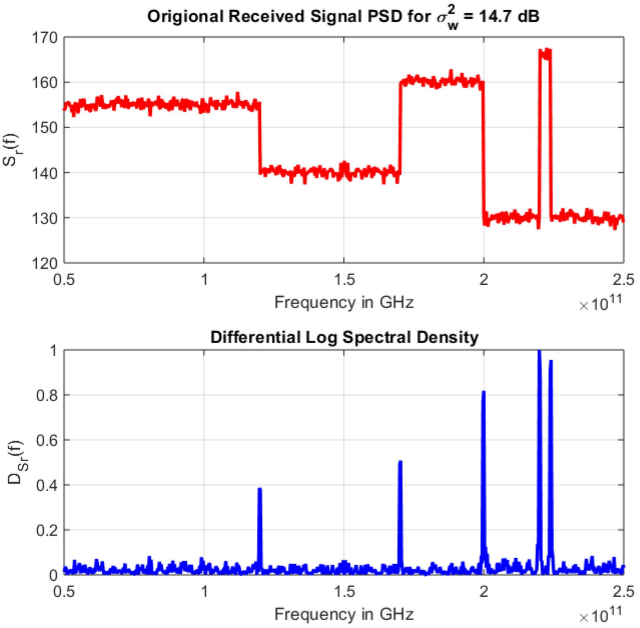

FIGURE 5. The spectral edges when applying the proposed DLSD algorithm for the high SNR case (the average SNR is 5.9 dB for $\sigma_w^2 = 14.7$ dB).

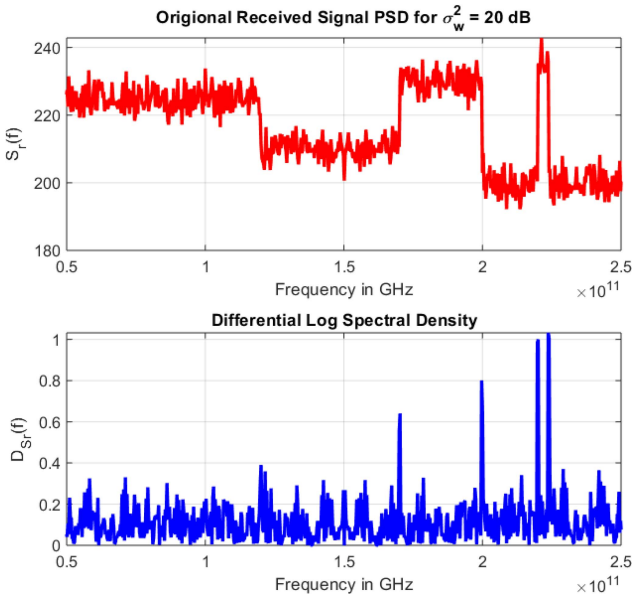

FIGURE 6. The spectral edges when applying the proposed DLSD algorithm for the medium SNR case (the average SNR is 0.6 dB for $\sigma_w^2 = 20$ dB).

In fact, the performance of the TVD-MM algorithm is affected by the choice of the regularity parameter as well as the number of iterations taken by the TVD-MM algorithm to converge. According to our assumptions on the wideband spectrum scenario, it becomes adequate to apply the TVD-MM algorithm over about 10 iterations to reduce the spurious edges and to significantly identify the spectral boundaries if $\sigma_w^2 > 20$ dB (i.e., the average SNR < 0 dB). In this case, the elapsed time measured for 10 iterations was 0.357 sec on a Intel Core i7-8550U processor (1.8 GHz), with a R2018a MATLAB program. On the other

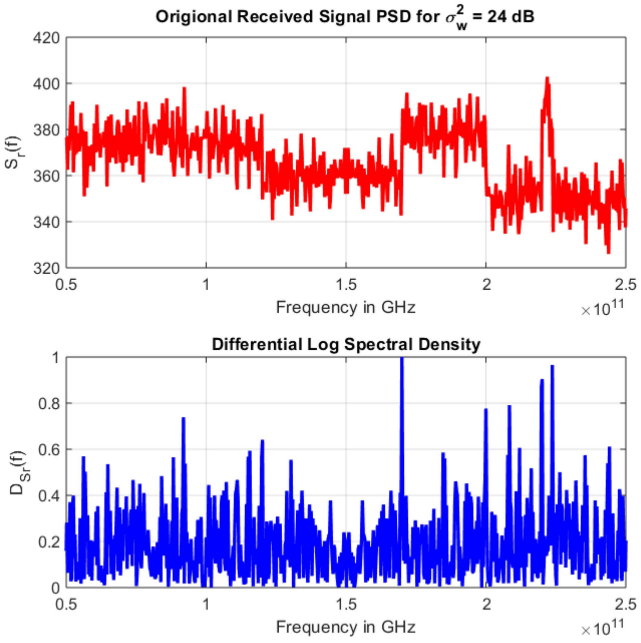

FIGURE 7. The spectral edges when applying the proposed DLSD algorithm for the low SNR case (the average SNR is −3.4 dB for $\sigma_W^2 = 24$ dB).

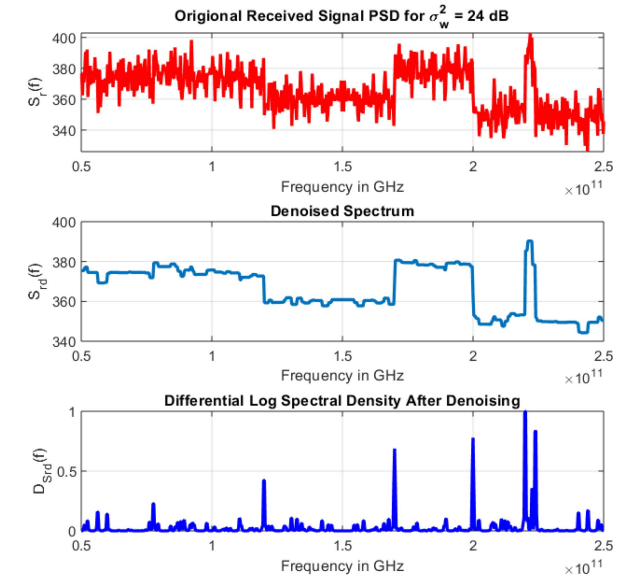

FIGURE 8. The spectral edges when applying the proposed DLSD algorithm with denoising for the low SNR case (the average SNR is −3.4 dB for $\sigma_W^2 = 24$ dB).

hand, the elapsed time measured for employing the WTMM edge detection algorithm under the same simulation conditions was approximately 7 sec. Thus, in accordance with our application and the stated wideband criterion, the processing time of the DLSD after applying the denoising technique is much lower than that of the WTMM algorithm. The results of several Monte Carlo simulations for the DLSD algorithm are shown in Section V.

2) NOISE CHARACTERISTIC IN THE DLSD TECHNIQUE

In our cepstrum-based edge detection approach, differential cepstral peaks may arise not only due to the exact spectral

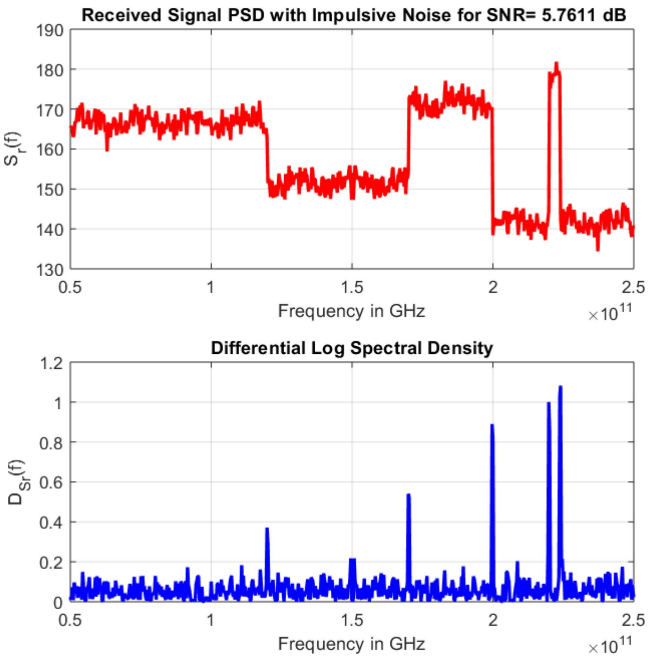

FIGURE 9. The spectral edges when applying the proposed DLSD algorithm if impulsive noise is imposed at average SNR of 5.7 dB.

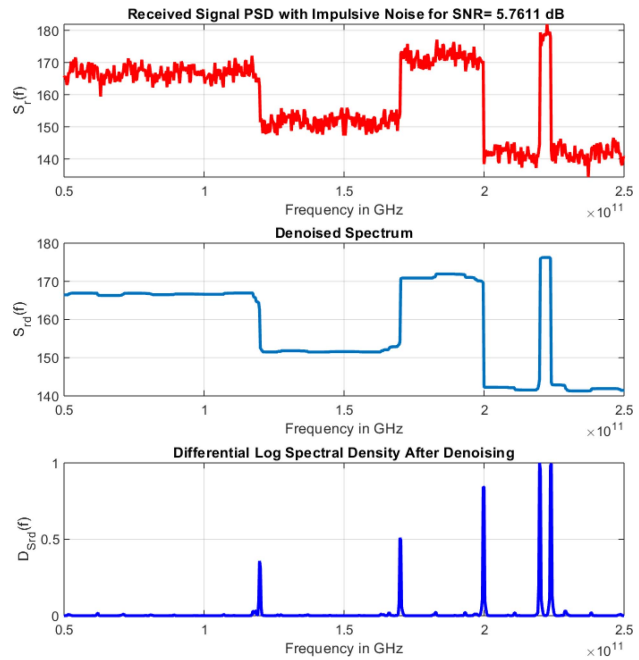

FIGURE 10. The spectral edges when applying the proposed DLSD algorithm with denoising if impulsive noise is imposed at average SNR of 5.7 dB.

edges but also due spurious edges generated from AWGN, impulsive noise, or very-NarrowBand Interference (vNBI). Therefore, it is important to identify the degrading effect of these sources on the target wide spectrum as follows:

- Concerning the ambient noise, we find that the effect of the AWGN in our DLSD technique is not harmful when it is applied in a high-to-medium SNR environment. Also, when denoising is employed before the DLSD

technique, the spectral edges became more recognizable in a low SNR environment.

- In wideband CR receivers, the impulsive noise and vNBI occur as narrow peaks in a spectral hole. Thus, it is desired not to identify these peaks during spectrum sensing. In Fig. 9, we illustrate the effect of applying the DLSD technique to the target wide spectrum for an average SNR of 5.7 dB and we find that the spectral peaks can be easily identified. Further, we applied the DLSD technique after denoising the spectral fluctuations and we find that the spectrum is smoothed out while the spectral boundaries are well recognized as shown in Fig. 10. Practically, some wideband receivers have a built-in capability to handle vNBI [18].

3) DESIGN CHARACTERISTICS OF DLSD EDGE DETECTOR

In our devised edge detection algorithm, the peak function evaluates its value at each sample point. In this case, all the positive sample points are candidate peaks. In order to reduce the effect of false peaks, we need to rule out these peaks based on their statistical distribution. Therein, we analyze the statistical characteristics of the peak function defining the DLSD approach. For the case of a baseband Binary Phase Shift Keying (BPSK) signal occupying the wideband of interest, the PSD of the BPSK signal is given by [34]:

$$S_x(f) = T_d^2 sinc^2(T_d f) \tag{15}$$

where T_d denotes the symbol duration. The peak function, based on the DLSD approach described in (12), is given by:

$$\mathcal{P}(f) = |D(f)| = \left| \frac{\frac{d}{df} S_r(f)}{S(f) + S_w(f)} \right| \tag{16}$$

in this case, if the noise at the CR receiver is assumed to be real Gaussian and based on (1), the estimate of $S_w(f)$ follows a Chi-squared distribution, $\chi^2_{(1)}$, with one degree of freedom. Accordingly, the edge detection problem can be formulated as a binary hypothesis test by:

$$\mathcal{P}(f) = \begin{cases} \mathcal{P}_0(f) = |\frac{\frac{d}{df} S_r(f)}{S_w(f)}| : & Under\ H_o \\ \mathcal{P}_1(f) = |\frac{\frac{d}{df} S_r(f)}{S(f)+S_w(f)}| : & Under\ H_1 \end{cases} \tag{17}$$

where $\mathcal{P}_0(f)$ is the set of spurious edges due to noisy spectral fluctuations, and $\mathcal{P}_1(f)$ is the set of noisy spectral boundaries. In order to design the detector, we need to find the detection threshold based on the distribution of (17) under the null hypothesis. In this case, we must obtain the right-tail probability of the proposed test statistic under H_0 for a fixed value λ of the false alarm probability denoted by P_{FA} [35]:

$$P_{FA} = \int_{\{\mathcal{P}:\mathcal{T}>\eta\}} f_{\mathcal{P}}(\mathcal{P}; H_0)\ d\mathcal{P} = \lambda \tag{18}$$

where $\mathcal{T}$ is the detector test statistic, η is the detection threshold, λ is the P_{FA} value, and $f_{\mathcal{P}}(\mathcal{P}; H_0)$ is the probability density function of every peak value defined based on the peak function $\mathcal{P}(f)$. In other words, the detector test statistic is defined by:

$$\mathcal{T}[\mathcal{A}] = \{\mathcal{A}[i],\ if\ \mathcal{A}[i] \underset{H_0}{\overset{H_1}{\gtrless}} \eta\};\ 1 < i < L \tag{19}$$

where $\mathcal{A}[i]$ represents each peak value within the set of peaks of length L_p points defined in the quefrency domain. For positive peak values, we find that the statistical distribution of each point in $\mathcal{P}(f) = |D(f)|$ follows also χ^2_1, which is defined by:

$$f_{\mathcal{A}}(a) = \frac{\exp(-\frac{a}{2})}{\sqrt{2a\pi}},\ a > 0 \tag{20}$$

then by solving for (18), we obtain[2]:

$$P_{FA} = \frac{2}{\sqrt{\pi}} Q(\sqrt{\eta}) \tag{21}$$

Thus, the threshold of the DLSD edge detector for a given false alarm probability is given by:

$$\eta = \left[Q^{-1}\left(\lambda \frac{\sqrt{\pi}}{2} \right) \right]^2 \tag{22}$$

To sum up, the DLSD edge detection algorithm is illustrated as Algorithm 1.

Algorithm 1 DLSD Edge Detection Algorithm

```
Input: P(f), L_p, λ, η
Output: O // set of detected edges
Begin O = ∅ // initially empty set
for (i = 1; i < L_p; i++) do
A[i] = P(f, L_p, i, |D(f)|_i)
if A[i] > η then
    O = O ∪ A[i]
end if
end for
```

B. THE DETECTION OF NOISE-LIKE PU SIGNALS BY DIFFERENT CEPSTRAL APPROACHES

Following the edge detection process, we proceed by introducing novel PU detection techniques for detecting the presence of noise-like signals in the case of the single-band and the multiband spectrum sensing scenarios.

1) IMPROVED PB-ACD TECHNIQUE BY SIGNAL SMOOTHING

In the PB-ACD technique, we estimate the autocorrelation of the received wideband signal and then evaluate the cepstrum. To enhance the detector performance, we aim to reduce the fluctuations experienced in the ACE before evaluating the PSD of the received signal. The functional block diagram of the smoothing process is shown in Fig. 11. In the literature, there are many methods employed for signals denoising

2. The function $Q(.)$ describes the tail probability of the standard normal distribution; $Q(x) = \frac{1}{\sqrt{2\pi}} \int_x^\infty \exp(-\frac{t^2}{2}) dt$.

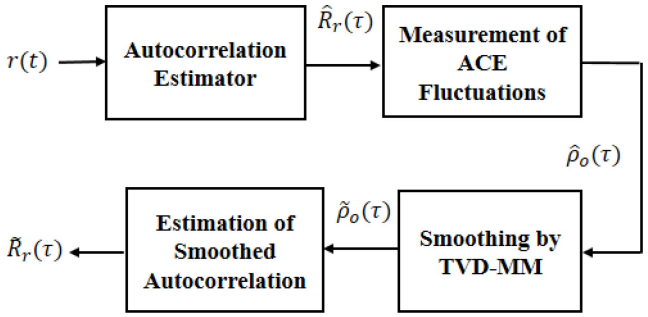

FIGURE 11. The proposed smoothing process; $\hat{R}_r(\tau)$ is the autocorrelation estimate of the received signal; $\hat{\rho}_o(\tau)$ is the ACE fluctuations; $\tilde{\rho}_o(\tau)$ is the smoothed ACE fluctuations; $\tilde{R}_r(\tau)$ represents the smoothed autocorrelation estimate.

which includes linear, Wiener, and wavelet-based filtering. In these approaches, the noisy received signal is being processed provided that prior knowledge of the noise statistics and the transmitted signal shape is available. However, in a non-cooperative semi-blind CR context, this information is not available so the conventional techniques would fail especially in the case of noise-like signals.

Recently, variational calculus has been employed in modern communication systems and statistical signal processing for different purposes such as choosing an optimal signaling function and deciding on certain statistical distributions that minimizes Fisher's information [36]. Moreover, variational methods have drawn great interest in solving image processing problems that including image denoising and deblurring [37]. Our choice to process the fluctuations of the ACE rather than the autocorrelation itself or the noisy observed time-domain signal is motivated by the following:

- Denoising a SS signal in the time domain without having prior information about the coding pattern is a difficult task and could fail due to its similarity with noise.
- Analysis of an underlying signal using its autocorrelation provides a means to enhance significant patterns that identify the signal.
- It has been shown in the work of Burel in [16] that the fluctuations of ACE of noise differ from that of a spread spectrum signal. This distinguishing feature can be applied to eliminate the noisy variation in the autocorrelation of the received SS signal.

In order to compute the autocorrelation estimator, we can divide the received time domain signal into M segments over a time rectangular window of a duration T. Then, we can evaluate the ACE for the m^{th} segment by [16]:

$$\hat{R}_r^m(\tau) = \frac{1}{T}\int_0^T r(t)r^*(t-\tau)dt \tag{23}$$

where $r^*(t)$ denotes the complex conjugate of the received signal, and τ is the time lag. In the statistical description of random processes, the second order moment describes the random fluctuations of a signal. Since the variance may characterize the random fluctuations around the mean value, the fluctuations of the ACE are identified by their mean and variance as mentioned in [16]. The measure of the fluctuations in terms of the second order moment of the ACE is given by:

$$\hat{\rho}_{R_r}(\tau) = \left\langle |\hat{R}_r(\tau)|^2 \right\rangle \tag{24}$$

or approximately,

$$\hat{\rho}_{R_r}(\tau) = \frac{1}{M}\sum_{m=0}^{M-1}\left|\hat{R}_r^m(\tau)\right|^2 \tag{25}$$

where $< . >$ in (24) represents the averaging operator. If the signal and noise are considered uncorrelated then we get:

$$\hat{R}_r(\tau) \approx \hat{R}_s(\tau) + \hat{R}_w(\tau) \tag{26}$$

where $R_s(\tau)$ and $R_w(\tau)$ are the autocorrelation of the noise-free signal and the noise at the CR receiver, respectively. In this case, we can define the underlying fluctuations of the ACE of the received signal according to (26) by:

$$\hat{\rho}_{R_r}(\tau) = \hat{\rho}_x(\tau) + \hat{\rho}_w(\tau) \tag{27}$$

a) *Fluctuations smoothing by the TVD-MM algorithm:* In general, the variational calculus is employed to find local extrema in a functional by solving differential equations. Signal denoising is one of its essential applications [38]. An important aspect of signal denoising is to preserve signal features, and also identify signal trends. An approach for the signal denoising by variational calculus is the TVD, through which the output is obtained by minimizing a particular cost function. Unlike conventional filtering, the TVD is defined in terms of an optimization problem. To formulate our smoothing problem, we should illustrate first the following notations:

- The $L-$point signal $\hat{\boldsymbol{\rho}}_{\boldsymbol{s}}$ is represented by the vector:

$$\hat{\boldsymbol{\rho}}_{\boldsymbol{s}} = \left[\hat{\rho}_s(0), \ldots, \hat{\rho}_s(L-1)\right]^T \tag{28}$$

- The ℓ_1 norm of the vector $\boldsymbol{d}$, which represents the discrete notations of the continuous variable t, is given by:

$$||\boldsymbol{d}||_1 = \sum_{\ell}|d(l)| \tag{29}$$

- The ℓ_2 norm of the vector $\boldsymbol{d}$ is given by:

$$||\boldsymbol{d}||_2 = \left[\sum_{\ell}|d(l)|^2\right]^{\frac{1}{2}} \tag{30}$$

- The diagonal matrix $\boldsymbol{D}$ is given by:

$$\boldsymbol{D} = \begin{bmatrix} 1 & 0 & 0 & 0 \\ -1 & 1 & 0 & 0 \\ 0 & \ddots & 1 & 0 \\ 0 & 0 & -1 & 1 \end{bmatrix}$$

by which the first-order difference of a $L-$point signal $\hat{\boldsymbol{\rho}}_{\boldsymbol{s}}$ is denoted by: $\boldsymbol{D}\hat{\boldsymbol{\rho}}_{\boldsymbol{s}}$

- The measurement of the total variation of a $L-$point signal $\hat{\boldsymbol{\rho}}_{\boldsymbol{s}}$ is given by [39]:

$$TV(\hat{\boldsymbol{\rho}}_{\boldsymbol{s}}) = \sum_{l=1}^{L-1} \left|\hat{\rho}_s(l) - \hat{\rho}_s(l-1)\right| = \left|\left|\boldsymbol{D}\hat{\boldsymbol{\rho}}_{\boldsymbol{s}}\right|\right|_1 \quad (31)$$

- The optimization problem, defining the smoothing of the ACE fluctuations, is given by:

$$\hat{\rho}_s(l) = arg \min_{\hat{\rho}_s(l)} \{F\big(\hat{\rho}_s(l)\big)\} \quad (32)$$

where $F(.)$ is the functional to be minimized in order to find the desired estimate. This functional can be defined in terms of mean squared error, such as [39]:

$$F\big(\hat{\rho}_s(l)\big) = \frac{1}{2}\sum_{l=0}^{L-1} \left|\hat{\rho}_o(l) - \hat{\rho}_s(l)\right|^2 + \alpha TV\big(\hat{\boldsymbol{\rho}}_{\boldsymbol{s}}\big) \quad (33)$$

where L is the maximum time lag at which the ACE fluctuations function is evaluated, $\hat{\rho}_o(l)$ denotes the observed fluctuations, for the case of uncorrelated signal and noise, that is given by:

$$\hat{\rho}_o(\tau) = \hat{\rho}_s(\tau) + \hat{\rho}_w(\tau) \quad (34)$$

and $\alpha > 0$ represents the regularization parameter that controls the smoothing degree. An appropriate value of α can be found heuristically.

In order to solve the minimization problem defined in (32), various algorithms can be employed, such as the TVD clipping algorithm [40]. However, the appropriate choice of an algorithm depends on the desired accuracy level and the convergence rate. For example, the Majorization-Minimization (MM) algorithm is applied to solve the TVD problem, which provides a significant accuracy on the expenses of the convergence time. The MM algorithm solves the minimization problem using a sequence of functions, called majorizer functions, that are easier to solve than the original cost function. To use the MM algorithm and reduce the computation burden, one must choose carefully an optimization function denoted by $G(\hat{\boldsymbol{\rho}}_{\boldsymbol{s}})$ to approximate $F(\hat{\boldsymbol{\rho}}_{\boldsymbol{s}})$. To choose $G(.)$, the MM approach requires that:

1) $G(\hat{\boldsymbol{\rho}}_{\boldsymbol{s}})$ is a majorizer of $F(\hat{\boldsymbol{\rho}}_{\boldsymbol{s}})$: $G(\hat{\boldsymbol{\rho}}_{\boldsymbol{s}}) \geq F(\hat{\boldsymbol{\rho}}_{\boldsymbol{s}}), \forall \hat{\rho}_s(l)$.
2) The majorizer coincides with the $F(.)$ at each iteration k: $G_k(\hat{\rho}_s(l)) = F(\hat{\rho}_s(l))$.
3) $G(\hat{\boldsymbol{\rho}}_{\boldsymbol{s}})$ must be a convex function, so that the MM algorithm obtains the solution at each k^{th} iteration by minimizing the majorizer function.

b) *Application of the proposed smoothing process to the case of detection a DS-SS signal:* To anticipate a constructive example for showing the applicability of the proposed smoothing process to our detection problem, consider the case of a passband DS-SS signal, $s(t)$, occupying a wideband of interest with the autocorrelation function given by [40]:

$$R_s(\tau) = \frac{A^2}{2} R_d(\tau) R_p(\tau) cos(2\pi f_c \tau) \quad (35)$$

where $R_d(\tau)$ and $R_p(\tau)$ are the autocorrelation of the data and spreading waveform, respectively,[3] and they are given by [40]:

$$R_d(\tau) = \Lambda\left(\frac{\tau}{T_d}\right) = \frac{1-|\tau|}{T_d}$$
$$R_p(\tau) = -\frac{1}{N_s} + \frac{N_s+1}{N_s}\sum_{i=-\infty}^{\infty} \Lambda\left(\frac{\tau - iN_sT_c}{T_c}\right) \quad (36)$$

Based on the baseband version of (35), we can express the ACE fluctuation function of $s(t)$ by:

$$\hat{\rho}_s(\tau) \approx \rho_p \sum_{i=-\infty}^{\infty} \Lambda\left(\frac{\tau - iN_sT_c}{T_c}\right) \quad (37)$$

in which $\hat{\rho}_s(\tau)$ viewed as a periodic triangular wave form with peak values ρ_p. According to (37), a convenient majorizer function at the k^{th} iteration $G_k(\hat{\rho}_s(\tau)) = g(t)$ for one period of $\hat{\rho}(\tau)$ is given by:

$$g(t) = c - bt^2 \quad (38)$$

From the MM algorithm, $g(t)$ must satisfy:

$$g(t) \geq f(t), \ \forall t \quad (39)$$

where $f(t)$ is the original cost function. Equivalently, if we set $\rho_p = 1$, then we should have:

$$c - bt^2 \geq \frac{1-t}{T_c}, \ \forall t > 0 \quad (40)$$

In this case, we need to evaluate the constants c and b to validate that the chosen function in (38) is a majorizer. The mathematical analysis to find c and b yields the following:

$$b = \frac{1}{2T_c|t_k|}, \quad c = \frac{1-2|t_k|}{2T_c} \quad (41)$$

See Appendix A for the proof.

Clearly, an upper bound of one period of $f(t)$ is given by $g(t)$, then by substituting c and b in (40), we get:

$$\frac{1-2t_k}{2T_c} - \frac{t^2}{2T_c t_k} \geq \frac{1-|t|}{T_c}, \ \forall t \in \mathbb{R} \quad (42)$$

To obtain the required cost function, we use $d(l)$ for the discrete notation instead of t, and then by summing over l, we obtain:

$$\sum_{l=1}^{L}\left(\frac{1-2|d_k(l)|}{2T_c} - \frac{d^2(l)}{2T_c|d_k(l)|}\right) \geq \sum_{l=1}^{L}\frac{1-|d(l)|}{T_C} \quad (43)$$

By using vector notations, we can rewrite (43) in a compact form as:

$$\left(-\frac{N}{2} - ||\boldsymbol{d}_k(l)||_1 - \frac{1}{2}\boldsymbol{d}^T\boldsymbol{\Delta}_k^{-1}\boldsymbol{d}\right) \geq -||\boldsymbol{d}||_1 \quad (44)$$

where $\boldsymbol{\Delta}_k = diag(|\boldsymbol{d}_k(l)|)$ denotes a diagonal matrix. Recalling the definition of the TVD in (31), then by replacing

3. T_d is the symbol duration, T_c is the chip duration, Λ is the triangular function; $N_s = 2^{m_s} - 1$ is the length of the m-sequence pseudo random spreading code; m_s is the degree of a chosen primitive polynomial.

$\boldsymbol{d}$ with $\boldsymbol{D}\hat{\boldsymbol{\rho}}_s$ in (44), multiplying it by the regularity parameter α, and adding the error data term $e_r(l) = \frac{1}{2}||\hat{\rho}_o(l) - \hat{\rho}(l)||_2^2$ to its both sides, then we get:

$$e_r(l) + \frac{-\alpha N}{2} - \alpha \left\|\boldsymbol{D}\hat{\boldsymbol{\rho}}_{s_k}(l)\right\|_1 - \frac{\alpha}{2}\hat{\boldsymbol{\rho}}_s^T \boldsymbol{D}^T \boldsymbol{\Delta}_k^{-1} \boldsymbol{D}\hat{\boldsymbol{\rho}}_s \geq e_r(l) - \alpha \left\|\boldsymbol{D}\hat{\boldsymbol{\rho}}_s\right\|_1 \quad (45)$$

Clearly, the majorizer of the cost function is given by:

$$G_k\left(\hat{\boldsymbol{\rho}}_s\right) = e_r(l) + \frac{-\alpha N}{2} - \alpha ||\boldsymbol{D}\hat{\boldsymbol{\rho}}_{s_k}(l)||_1 - \frac{\alpha}{2}\hat{\boldsymbol{\rho}}_s^T \boldsymbol{D}^T \boldsymbol{\Delta}_k^{-1} \boldsymbol{D}\hat{\boldsymbol{\rho}}_s \quad (46)$$

Using (46), we seek to obtain the update equation $(\hat{\boldsymbol{\rho}}_s)_{k+1}$ as follows:

- Set the iteration index k to 0 and initialize $(\hat{\rho}_x)_0$.
- Set $(\hat{\rho}_x)_{k+1}$ as a minimizer of $G_k(\hat{\rho}_x)$ such that:

$$(\tilde{\rho}_x)_{k+1} = arg \min_{\hat{\rho}_x} \; G_k(\hat{\rho}_x) \quad (47)$$

- Set $k = k + 1$ and go to step 2.

Accordingly, by differentiating (46) and equating the results to zero, it yields:

$$(\tilde{\rho}_x)_{k+1} = (\boldsymbol{I} + \boldsymbol{U})^{-1} \hat{\boldsymbol{\rho}}(\boldsymbol{l}) \quad (48)$$

where $\boldsymbol{I}$ is the identity matrix, and $\boldsymbol{U}$ is defined by:

$$U = \alpha \boldsymbol{D}^{\boldsymbol{T}} \boldsymbol{\Delta}_{\boldsymbol{k}}^{-\mathbf{1}} \boldsymbol{D} \quad (49)$$

In Fig. 12, Fig. 13, and Fig. 14, we illustrate the effect of applying the smoothing process for the case of a DS-SS signal at SNR of -10 dB. The operating specifications are based on the IEEE802.11a standards that use the DS-SS signal with 5 GHz as the operating frequency and 54 Mbps for the data rate [41]. It is important to clarify that despite the effective results provided by the proposed smoothing process on the estimated PSDs, there is an 8% estimation error in the operating frequency. For this reason, it is essential that the PU detector operates independently on the operating frequency value.

Taking into account that random ACEs fluctuations of the DS-SS signal and that of the AWGN are distinguishable, the smoothed PB-ACD exploits the advantage of denoising the fluctuations of the Autocorrelation Estimators (ACEs) by the TVD-MM algorithm. The calculation of the ACEs fluctuations involves dividing the time domain signal into M segments as indicated in (25). By respecting Nyquist's rate f_{s_N}, the estimated PSD maintains the exact frequency information. However, in the case of oversampling the signal, the estimated PSD experiences a minor loss of frequency localization [42].

As the number of samples increases within each signal segment, in case of oversampling, the summation of the segmented autocorrelation will smooth out the details of the signal. Therefore, the maxima presented in the sum will be more smoothed resulting in a minor frequency shift in the estimated PSD. Also, as the oversampling increases above double the Nyquist's rate, a substantial loss of frequency localization occurs, so the frequency error is not fixed and does not depend on the number of simulation trials.

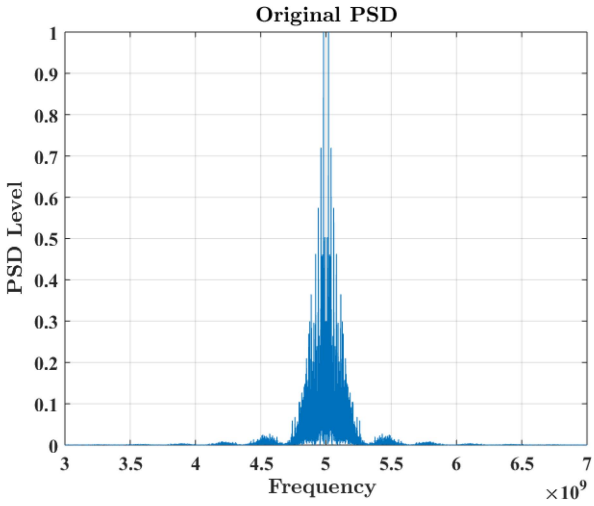

FIGURE 12. The original PSD of a DS-SS signal.

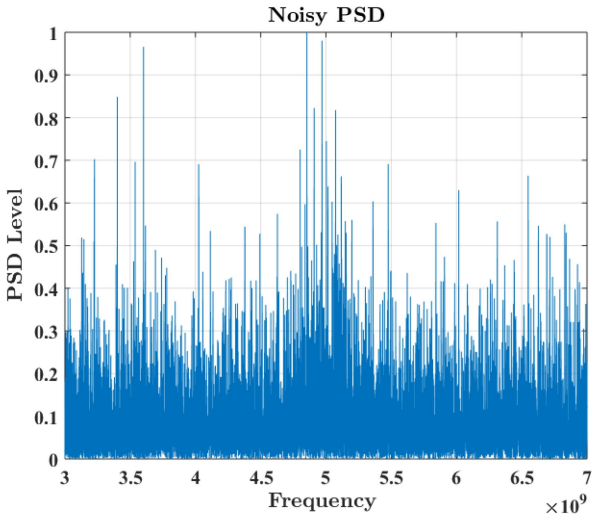

FIGURE 13. The received signal PSD at SNR of −10 dB.

Despite the fact that oversampling a time-domain signal is supposed to improve the process of estimating the autocorrelation, it is shown in [42] that oversampling short data sequences at Nyquist's rate increases the variance of the autocorrelation estimate such that the mean-squared error of the estimate increases. On the other hand, it is sufficient to sample at the Nyquist's rate for long data sequences (i.e., as in our presented case) such that the variance of the autocorrelation estimate attains its minimum value. To demonstrate the effect of varying the sampling rate in calculating the ACEs, Fig. 15 and 16 show the original and the noisy PSD of the PU signal and the estimated PSD after applying the smoothing process, respectively. When the signal is sampled at the Nyquist's rate, no loss of frequency localization is encountered as shown in Fig. 16.

The TVD employs the regularity parameter, α, to control the degree of smoothing. Increasing α gives more weight

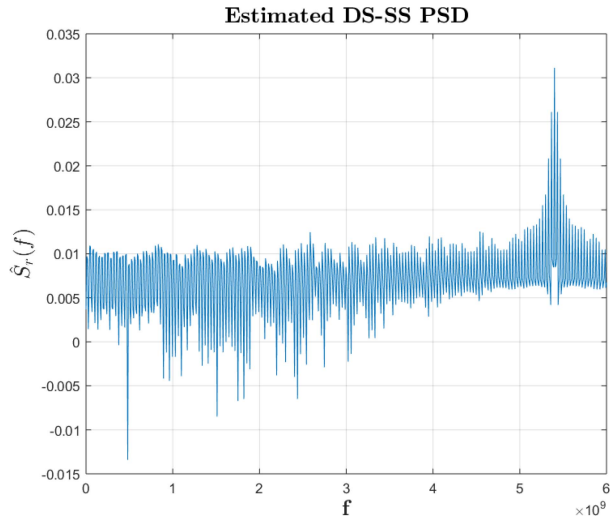

FIGURE 14. The estimated PSD $\hat{S}_r(f)$ in decibels after applying the TVD-MM algorithm to the fluctuations of the ACEs of the received signal in case of oversampling.

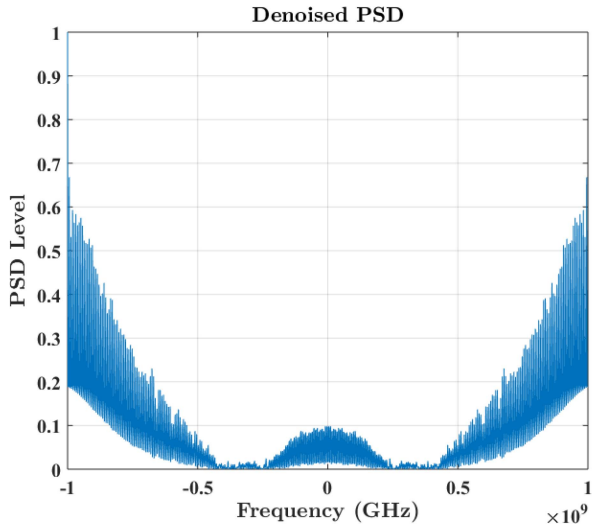

FIGURE 16. The estimated PSD after applying the TVD-MM algorithm to the fluctuations of the ACEs of the received signal; the signal is sampled at Nyquist's rate.

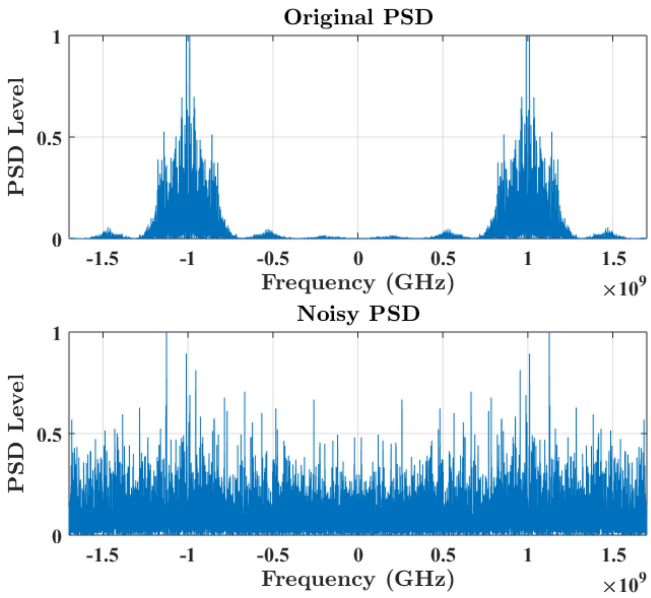

FIGURE 15. An illustrative example of the original PSD of the DS-SS signal and its noisy spectral density.

to the term that measures the fluctuations of the signal. In this case, choosing small values for the regularity parameter translates into reduced spectral fluctuations but may affect the level of the exact spectral boundaries. Therefore, before choosing the regularity parameter, we have to be aware of the required detection accuracy level to avoid over-smoothing the analyzed signal and hence increasing the misdetection probability.

2) THE PROPSED BB-ACD TECHNIQUE

The proposed BB-ACD consists of a CTF followed by the PB-ACD. The CTF utilizes the circular topology of a typical sinusoidal signal to separate the baseband signal or its squared version. The detection of a noise-like PU signal, or a conventional digitally modulated signal, by the PB-ACD technique, depends on the presence of a strong peak appearing at a quefrency value equivalent to the reciprocal of the center frequency of a certain subband. Due to the possible frequency estimation errors from the edge detection phase, the PB-ACD gives poor performance. Thus, our objective is to utilize the baseband features of the target signal appearing in the power cepstrum of the received signal. Specifically, we exploit the peaks reflecting the periodicity that appears in the power cepstrum of the n^{th} baseband signal. These peaks interpret the presence of digitally modulated symbols of a possible PU signal. By using the combination of the HF and the SLD, we can obtain the required term representing the baseband signal. A functional block diagram of the proposed BB-ACD is shown in Fig. 17. To illustrate the concept, we notice in Fig. 18 that the autocepstrum of a passband DS-SS signal reveals a major peak that appears at the reciprocal of the carrier frequency after getting the inverse Fourier Transform of the autocepstrum, whereas a periodicity is revealed in the baseband version of the signal's power cepstrum (i.e., the frequency domain version of the autocepstrum) in Fig. 19. This is shown at multiples of the reciprocal of the bit duration of the DS-SS signal.

To illustrate the calculus, consider a digitally modulated carrier signal, denoted by $B_d(t)$, is defined by:

$$B_d(t) = B(t)\ cos(2\pi f_c t) \tag{50}$$

where $B(t)$ is the baseband signal, and f_c is the carrier frequency (i.e., the center frequency of the n^{th} subband). By the Hilbert filtering applied to (50), the output $O(t)$ of the CTF is given by:

$$O(t) = B_d^2(t) + \left[B_d^H(t)\right]^2 = B^2(t) \tag{51}$$

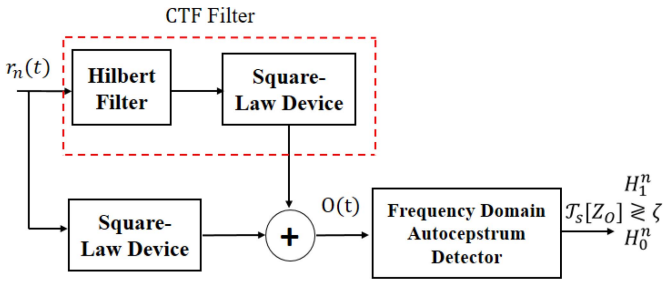

FIGURE 17. The system architecture of the proposed baseband autocepstrum technique.

where H denotes the Hilbert version. Practically, the carrier frequency will be replaced with $f_e = f_c \pm \delta f$, where f_e indicates the estimated center frequency, and δf is the frequency deviation from the actual carrier frequency that causes the estimation error. Also, the noise effect at the CR receiver is considered for the AWGN noise $w(t)$, hence, the output $O(t)$ becomes:

$$\begin{aligned} O(t) &= [B_d(t) + w(t)]^2 + \left[B_d^H(t) + w^H(t)\right]^2 \\ &= B_s(t) + \mathcal{E}_s(t) + 2B(t)\big[w(t)cos(2\pi f_c t) \\ &\quad + w^H(t)sin(2\pi f_c t)\big] \end{aligned} \quad (52)$$

In (52), the squared baseband version of the signal is denoted by $B_s(t) = B^2(t)$, and $\mathcal{E}_s(t) = w^2(t) + (w^H(t))^2$ denotes the squared envelope of the noise signal. However, it is required to eliminate the high frequency terms before defining the detector test statistic. A possible solution is to apply the autocepstrum approach for the case of uncorrelated noise and signal. To do this, first, we determine the autocorrelation of $O(t)$ such that:

$$R_O(\tau) \approx R_{B_s}(\tau) + R_{\mathcal{E}_s}(\tau) \quad (53)$$

then, by getting the Fourier Transform of $R_O(\tau)$, we obtain the corresponding PSD terms by:

$$S_O(f) \approx S_{B_s}(f) + S_{\mathcal{E}_s}(f) \quad (54)$$

By taking the natural logarithm of $S_O(f)$, we get the autocepstrum by:

$$Z_O(f) = \log\big[S_{B_s}(f) + S_{\mathcal{E}_s}(f)\big] \quad (55)$$

Since the BB-ACD utilizes the periodicity that may occur in the log-PSD of the received signal, we need to show at the beginning that the $S_{B_s}(f)$ is periodic in the cepstral domain, and then consider the noisy periodicities in $Z_O(f)$ due to the spectral fluctuations from $S_{\mathcal{E}_s}(f)$. Consequently, this periodic feature can be utilized to formulate the detector test statistic. In order to generalize the BB-ACD approach to digitally modulated signals, consider the following baseband version of (4) which is defined by:

$$B(t) = \sum_{k=-\infty}^{\infty} b_k p(t - kT_s) \quad (56)$$

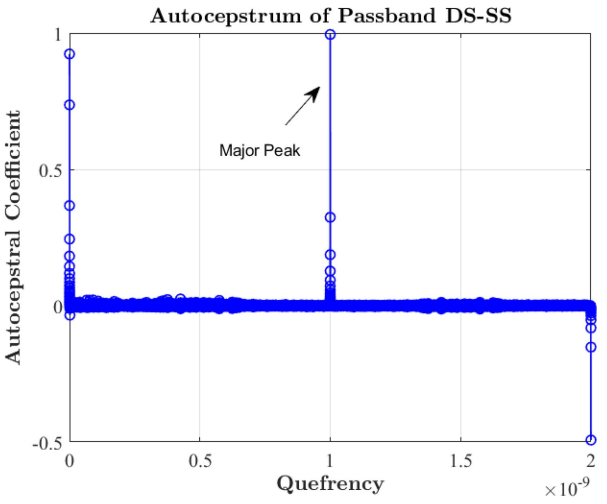

FIGURE 18. The autocepstrum of the passband DS-SS signal; a large peak is located at a quefrency value that is equivalent to the reciprocal of the signal's operating frequency of 1 GHz [15].

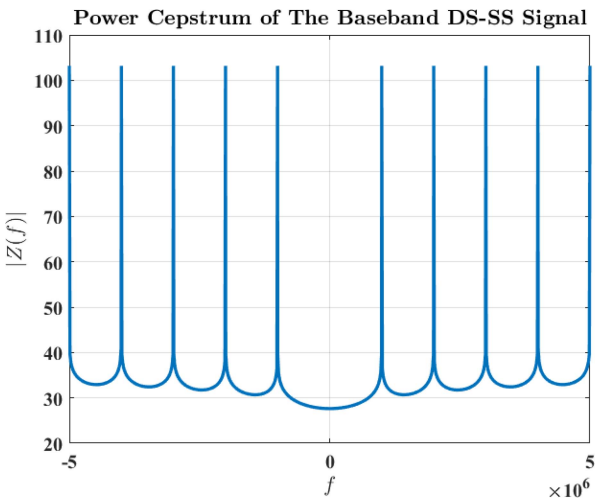

FIGURE 19. The frequency domain version of the autocepstrum of the baseband DS-SS signal which reveals periodicity at multiples of 1 MHz.

Conventionally, $B(t)$ is a polar signal and the pulse shape is the rectangular function $p(t) = \prod(t)$. Let us define the spectrum of $B_s(t)$ by $B_s(f) = |B(f)| * |B(f)|$, since we consider the magnitude of the spectrum, and the symbol $*$ denotes the convolution product. For a truncated binary sequence of size N_T, and with T_d being the symbol duration, $|B(f)| \approx N_T b_k P(f)$, where $P(f) = sinc(T_d f)$. We can obtain the required $B_s(f)$ from the time domain and then evaluating the Fourier transform to get:

$$B_s(f) \approx N_T^2 b_k^2 \ sinc^2(T_d f) \quad (57)$$

The natural logarithm of $B_s(f)$ results in a negative periodic function thus, in order to have a reliable detector test statistic, we choose to combine all periodic peaks appeared in $Z_O(f)$

by defining:

$$\mathcal{T}_s[Z_O] = \frac{1}{L_p}\sum_{i=1}^{L_p}|Z_O(i)| \tag{58}$$

where L_p is the number of peaks presented in the autocepstral signal. To devise a suitable detection threshold, we should find the statistical distribution of $\mathcal{T}_s$. Referring to (55), if the AWGN $w(t)$ is distributed as a Circularly Symmetric Complex Gaussian (CSCG) process, the squared-envelope of $w(t)$ is distributed as a $\chi^2_{(2)}$ process with two degrees of freedom, whose Probability Density Function (PDF) is given by [43]:

$$f_W(w) = \frac{1}{2}\exp(-w/2)\ , w > 0 \tag{59}$$

Thus, the statistical distribution of $\mathcal{T}$ follows a Modulus Log Chi-Squared (MLCS) (i.e., Modulus-log $-\chi^2_{(2)}$) distribution. By using the PDF approach of the transformation of random variables, the MLCS distribution is given by:

$$f_{\mathcal{T}_s}(t_s) = \frac{1}{2}\exp\left(t_s - \frac{1}{2}\exp(t_s)\right) + \frac{1}{2}\exp\left(-t_s - \frac{1}{2}\exp(-t_s)\right) \tag{60}$$

See Appendix B for the proof.

In order to get an expression for the detector threshold ζ, we follow the same concept indicated in (18) for a fixed false-alarm probability λ. By employing the method of substitution, we obtain:

$$\lambda = \exp\left(-\frac{\exp(\zeta)}{2}\right) - \exp\left(-\frac{\exp(-\zeta)}{2}\right) + 1 \tag{61}$$

also, we can simplify (61) by decomposing the exponential terms to obtain:

$$\lambda = \exp\left(-\frac{\exp(\zeta)}{2}\right) + 2\exp\left(-\frac{\exp(-\zeta)}{4}\right)\sinh\left(\frac{\exp(-\zeta)}{4}\right) \tag{62}$$

The approximation of the hyperbolic function can be given by Taylor's expansion. However, the Taylor series diverges to infinity, so a closed-form expression for ζ cannot be found analytically, and (62) can be solved numerically by different methods such as the Newton Raphson Method [44].

V. NUMERICAL RESULTS AND DISCUSSIONS

In order to validate the efficacy of the proposed wideband spectrum sensing approach, we begin with evaluating the performance of the proposed DLSD technique as opposed to different wavelet-based edge detection techniques. This evaluation includes calculating the average detection error probability P_e as mentioned in [14], which is given in terms of the probability of miss-detecting an actual spectral boundary P_{MD} and the probability of falsely detecting a spurious edge P_{FD}. Further, we evaluate the performance of the smoothed PB-ACD technique as opposed to the PB-ACD technique for detecting the presence of a possible noise-like signal. Then, we show the applicability of the proposed BB-ACD technique to different digitally modulated signals. We also address the problem of detecting noise-like signals by the PB-ACD technique under the carrier frequency uncertainty, and we show the advantage of applying the proposed BB-ACD instead.

A. PERFORMANCE EVALUATION OF THE PROPOSED EDGE DETECTION APPROACH:

The frequency of the wideband spectrum under consideration extends from 30 GHz to 300 GHz. The proposed algorithm is simulated through randomly generated spectrum models for generalization. The average PSD level within each occupied subband is maintained to 6 W/Hz assuming 60% of spectrum occupancy rate. Although the assumed average PSD level is large as opposed to normal radiation levels in practical settings, it is chosen to match the chosen specifications in [20] for the sake of comparison. The characteristics of each spectrum model are generated randomly. They include the number of subchannels within the wideband of interest, the exact spectral boundaries, and the signal power specified in each subband. These subbands are assumed to have different bandwidths to match up with the diversity of the transmission technologies.

Further, depending on the distance between the CR receiver and the transmission station in the occupied subband, as well as the status of the spectrum occupancy, the SNR level is assumed to differ from one subband to another. The performance of the proposed technique is tested by adding white Gaussian noise with the same power to the received RF stimuli corresponding to the whole sensed spectrum while maintaining the same average PSD level in all spectrum models.

The simulated PSD model is a modified version of the model presented in [18]. It is important to note that the modification is in the PSD shape; we assume a more practical raised-cosine approximation for the PSD shape rather than the ideal piecewise-constant shape widely employed. By referring to (5), $S_x(f)$ denotes the normalized PSD and we assume a raised-cosine pulse shape with a roll-off factor of 0.3. A summary of the simulation parameters is listed in Table 3. For clarification, Table 4 shows the detailed information of an example of a randomly generated PSD model shown in Fig. 20. The Simulations are done with R2018a MATLAB, and the obtained results are based on 1000 Monte Carlo trials.

First, we discuss the effects of applying the DLSD algorithm on spurious edges generated by the noisy spectral variations in P_{FD}. In Fig. 21, at considerably low-to-medium noise power (i.e., over the range [10, 22] dB), we notice that the proposed DLSD algorithm outperforms the WTMM, the WTMS, or the improved WTMM algorithms. Thanks to the ability of the cepstral analysis approach to reduce the noisy spectral variations. In fact, the white Gaussian noise's cepstrum becomes a Dirac impulse at the zeroth quefrency value.

TABLE 3. Simulation parameters for the edge detection technique.

Parameter/Tool	Description
Frequency Band	30-300 GHz
Spectral Estimation Method	Periodogram
Sample Size	1024
Number of PSD Models per Simulation	20
Spectrum Occupancy	60%
Average PSD Level in Occupied Channels	6 W/Hz
Noise Power	10 to 30 dB
Number of Monte Carlo Iterations	1000

TABLE 4. Spectral specifications of one randomly generated spectral model for $\sigma_w^2 =$ 20 dB.

Channel (N <15)	Boundaries (GHz)	Bandwidth (GHz)	PSD Level (W/Hz)	Signal Power (dB)	SNR
1	[30,36]	6	0	NA	NA
2	[36,142]	106	14.677	31.919	10.919
3	[142,190]	48	6.099	24.665	4.665
4	[190,224]	34	0	NA	NA
5	[224,240]	16	12.689	23.075	3.075
6	[240,300]	60	2.532	21.816	1.816

Clearly, this characterization of the AWGN in the cepstral domain helps in rejecting potential spurious edges. These results match the concluding insights from Fig. 5, Fig. 6, and Fig. 7. This means that the DLSD algorithm can characterize and reject the false edges.

From literature, the major drawback of the WTMM algorithm is the increased number of spurious edges which cannot be eliminated even with a threshold-based detection [14]. The superior performance of the WTMS technique over the WTMM technique is due to the averaging effect of the WTMS algorithm over the noisy spectral edges. However, as shown in Fig. 7, if the noise power increases (i.e., above 22 dB), the performance of the DLSD algorithm decreases due to the increased number of spurious edges. To improve the DLSD performance, we employed the TVD-MM algorithm in order to reduce the noisy fluctuations before applying the DLSD technique. We employed the TVD-MM algorithm on about 10 iterations with two different regularity parameters: $\alpha = 0.9$ and 1.2 respectively. As seen in Fig. 8 and 21, the employment of denoising before applying the DLSD algorithm helped in reducing the spurious edges and hence reducing the P_{FD}. Precisely, for a noise power value over the range [10, 22] dB, the DLSD algorithm with denoising outperforms the four considered algorithms and performs similar to the improved WTMM algorithm for $\sigma_w^2 > 22$ dB.

Considering the probability of miss-detecting and actual spectral boundary, the P_{MD} is plotted for the five considered algorithms in Fig. 22. We notice that the DLSD algorithm and the WTMS perform similarly over the noise power range [10, 18] dB. Since the WTMS algorithm enhances the wavelet modulus maxima that represent the spectral edges,

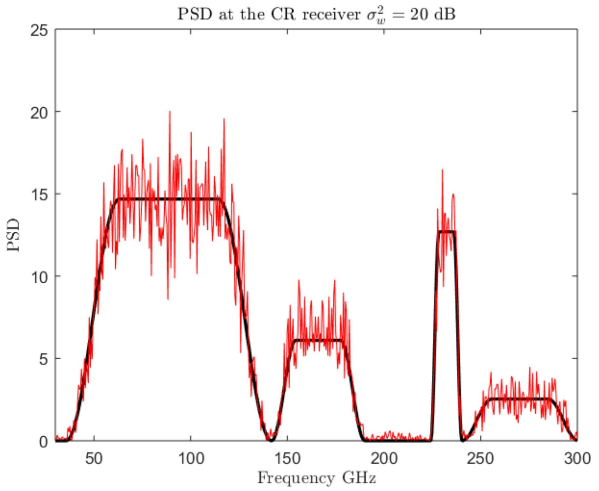

FIGURE 20. An example of a noisy spectral model.

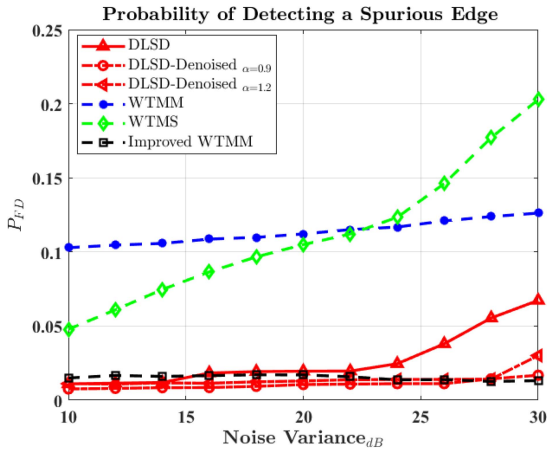

FIGURE 21. A comparison of the probability of false detection of an original edge by the DLSD technique evaluated as opposed to wavelet-based techniques.

it outperforms the WTMM and the improved WTMM techniques in this performance criterion. As the noise power increases above 18 dB, the DLSD algorithm falls behind the WTMS algorithm due to the lack of edge enhancement.

While the denoising effect of the DLSD technique reduces the false detection probability, it affects the miss-detecting probability as well. In other words, the suppression of noisy spectral fluctuations may result in suppressing a correct spectral boundary. This is due to the fact that the noisy spectral fluctuations tend to deform the actual spectral boundaries, so as the noise power increases, this deformations increases as well which cause the DLSD detector to reject some of the original subbands edges falsely. Remarkably, by using the DLSD algorithm in conjunction with the TVD-MM, the misdetection probability decreases and becomes the lowest among the probabilities of the other four considered algorithms for σ_w^2 up to 28 dB. Above the threshold of 28 dB, the WTMS algorithm has the lowest P_{MD}.

The average detection error probability is plotted for the five considered algorithms in Fig. 23. The proposed DLSD

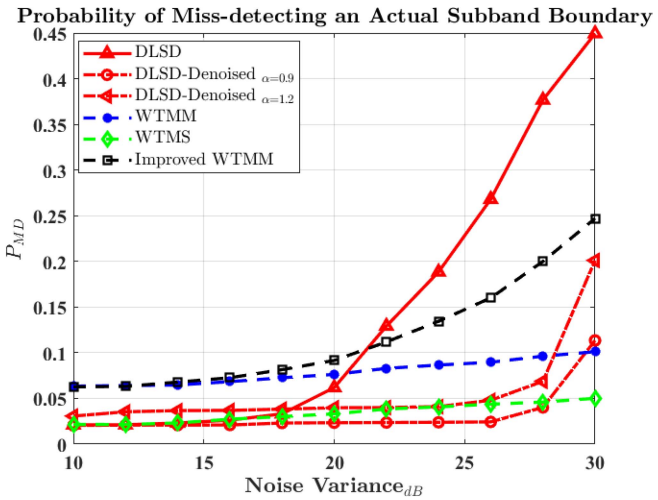

FIGURE 22. A comparison of the probability of misdetecting an original spectral boundary by the DLSD technique evaluated as opposed to wavelet-based techniques.

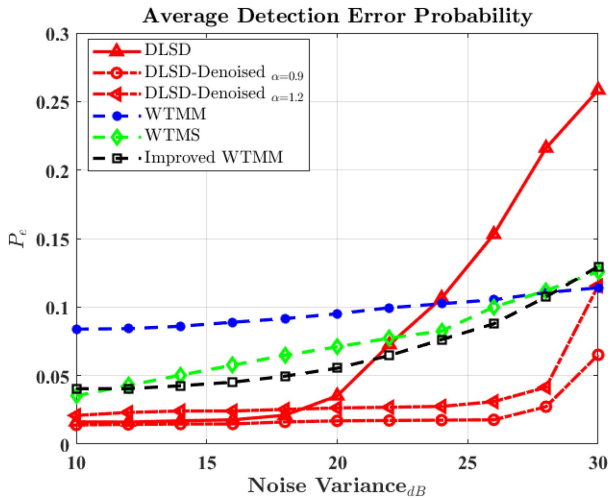

FIGURE 23. A comparison of the average detection error probability of the DLSD technique evaluated as opposed to wavelet-based techniques.

algorithm has a superior performance over the noise variance range of [10, 22] dB. The improved WTMM algorithm has a superior performance over the range [22, 28] dB. The proposed DLSD algorithm with denoising gives the best performance over the other considered algorithms when the noise power is above 28 dB. It is worth mentioning that the level of denoising offered by the TVD-MM algorithm is affected by the regularity parameter. Thus, this parameter must be chosen suitably according to the application to provide the required level of denoising and to avoid over smoothing which may diminish the characterization of the spectral boundaries. Moreover, Table 5 provides a comparison of the edge detection capability, the applicability, and the implementation complexity of the proposed approach under AWGN channel as opposed to the chosen wavelet-based techniques.

B. PERFORMANCE EVALUATION OF THE PROPOSED PU DETECTION TECHNIQUES

1) DETECTION OF NOISE-LIKE SIGNALS BY THE SMOOTHED PB-ACD TECHNIQUE

For the PU detection phase, different NBSS techniques can be employed. In the following, we start by reviewing the PB-ACD technique and compare it to the improved PB-ACD and other techniques. Our objective is to test the efficacy of the improved PB-ACD as an NBSS technique for the detection of noise-like signals such as DS-SS and IR-UWB signals.

In Section IV, we proposed a solution for improving the detection performance of the PB-ACD technique for detecting noise-like signals through a smoothing process. Indeed, the detection of low-power signals in CR is a spectrum sensing challenge, especially when the CR receiver has no knowledge of the specifications of the noise-like signal. The authors in [15] have evaluated the performance of the PB-ACD technique for detecting a DS-SS signal under the AWGN channel in the case of the SBSA. In this work, we aim to evaluate the performance of the smoothed PB-ACD in terms of the detection and the misdetection probabilities for two examples of noise-like signals, namely: a DS-SS signal and an Impulse Radio Ultra Wide Band (IR-UWB) signal. Our choice of the IR-UWB signal is due to its very low power level as compared to a typical narrowband RF signal and a spread spectrum signal.

The simulations are averaged over 3000 realizations with the following parameters for the DS-SS signal: the chip duration is 1.54 μsec. In the simulations, we employed a Boolean parameter Θ, which is uniformly distributed and takes randomly a value of 0 or 1 to include the presence or absence of a DS-SS PU signal. The used spreading code is based on a primitive polynomial defining the m-sequence code in the form of $x^6 + x + 1$. The length of the spreading code is 63 samples, and the sequence length of the analyzed signal is 4410 samples. The modulation type is the passband BPSK modulation scheme with a carrier frequency of 5 GHz, and a sampling frequency f_s of 30 GHz. The number of segments used to calculate the autocorrelation estimates in 630 segments, the regularity parameter α for the TVD-MM algorithm is set to 0.01 and the number of iterations is 10.

The performance measures are shown in Fig. 24 to Fig. 30. Fig. 24 shows the simulation results obtained in [15] for evaluating the detection probability of the PB-ACD technique as compared to the conventional ED technique for detecting the presence of a possible DS-SS signal. The simulations of the ED are carried on under the Central Limit Theorem (CLT) assumption and the noise statistics are estimated through histograms. The performance of the ED essentially depends on the settings of the detection requirements depending on the transmission standards. As shown in Fig. 24, at SNR of -15 dB, we find that the PB-ACD technique is superior to ED by approximately 40% for $P_{FA} = 0.01$ and by 20% for $P_{FA} = 0.05$. As the SNR increases slightly from -15 to -10 dB, the PB-ACD and the ED techniques behave similarly.

TABLE 5. Comparing wavelet analysis to cepstral analysis for edge detection in wideband spectrum sensing.

Approach	Wavelet Analysis	Cepstral Analysis
Post Processing	The Local maxima are found through differentiating the filtered PSD.	The Local maxima are found through differentiating the autocepstrum in frequency domain.
White Noise Characteristics	**WTMM**: calculates the wavelet modulus maxima in the frequency domain. However, the noise impact affects detection of spectral boundaries. **Improved WTMM**: exploits the singularity characteristics of the wavelet multiscale to identify spurious edges and reject them. Its performance is degraded in low SNR environment. **WTMP**: The product of the first derivative of WT is developed for noise suppression and edge sharpening, but it results in attenuating the edges due to the the multiplication operation. **WTMS**: It preserves the edges information and avoids edges attenuation. Increasing the scales leads to a better detection performance but at higher complexity.	**Time-domain Cepstrum and Autocepstrum**: The AWGN fluctuations are suppressed at all the quefrencies values except for a major peak at the zeroth quefrency at medium-to-high SNR values. **DLSD**: It reduces the noisy spectral variations.
Application Versatility	The detection performance depends on the analyzed signal and the used mother wavelet function.	The employment of the CA approach depends on the type of the cepstral algorithm used that is suitable for the problem under analysis to successfully reveal the hidden signal's features. Any cepstral algorithm may require further processing to achieve the required results.
Implementation Complexity	WT is implemented as a bank of filters. Reducing spurious edges can be accomplished by processing the signal of interest through all scales which substantially increases the computational burden.	Relatively lower than the wavelet approach.

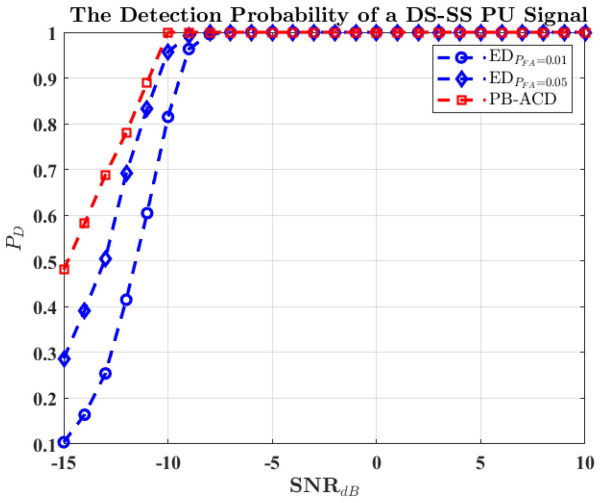

FIGURE 24. The detection probability of the PB-ACD as compared to that of the ED for detecting a DS-SS Signal.

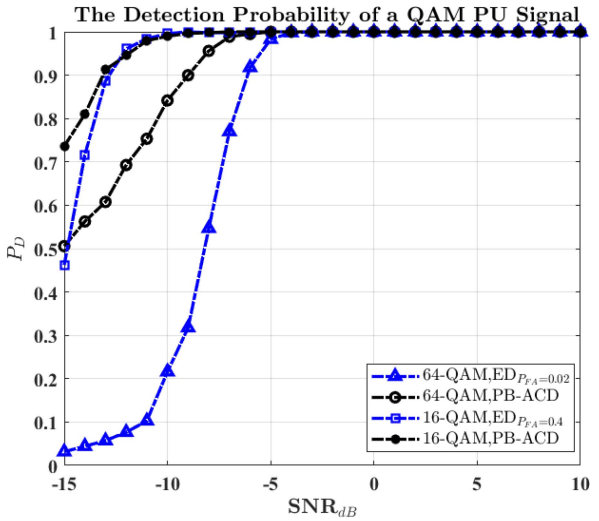

FIGURE 25. The detection probability of the PB-ACD as compared to that of the ED for detecting a QAM PU Signal.

Also, to elaborate more on higher-order and advanced modulations, Fig. 25 shows a comparison of the detection performance of the PB-ACD technique with ED for detecting 16-QAM and 64-QAM PU signals. In wireless communication, the 64-QAM modulation scheme is used in 4G systems in the uplink and provides the most benefit in small cell environments under good uplink conditions. Moreover, we simulated the PB-ACD technique, as shown in Fig. 26, to test its detection performance for detecting OFDM PU signals and compare them with ED and the Eigenvalue Detection (EVD). From Fig. 26, the detection performance of the PB-ACD technique outperformed the ED and EVD techniques in the SNR range $[-15, -6]$ dB. In simulating OFDM modulated signals, we considered the parameters defined in the IEEE802.11 specifications [29].

To provide more improvement over the ED technique, we applied the proposed smoothed PB-ACD technique and compare it with different state-of-the-art spectrum sensing techniques, such as the EVD, and the Matched Filter

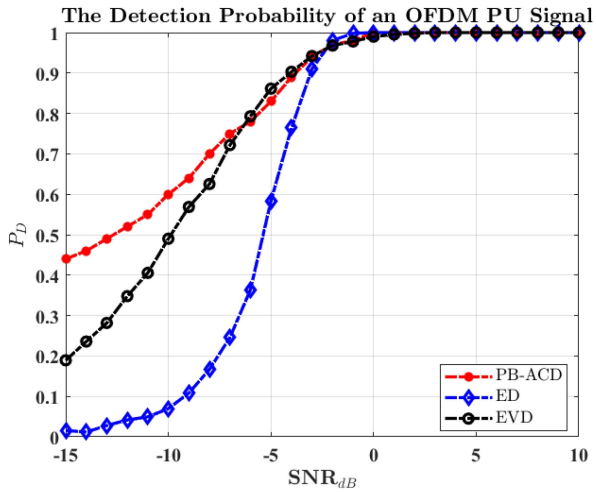

FIGURE 26. The detection probability of the PB-ACD as compared to that of the ED and EVD for detecting an OFDM PU Signal.

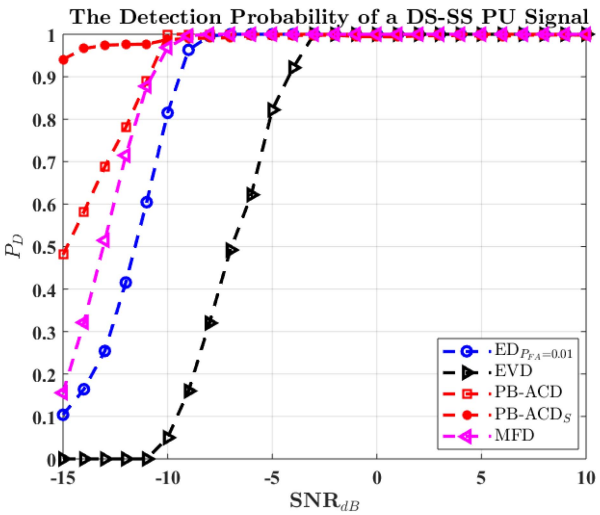

FIGURE 27. The detection probability of the PB-ACD as compared to the smoothed PB-ACD and different state-of-the-art techniques for detection a DS-SS signal; PB-ACD_S denotes the smoothed PB-ACD technique.

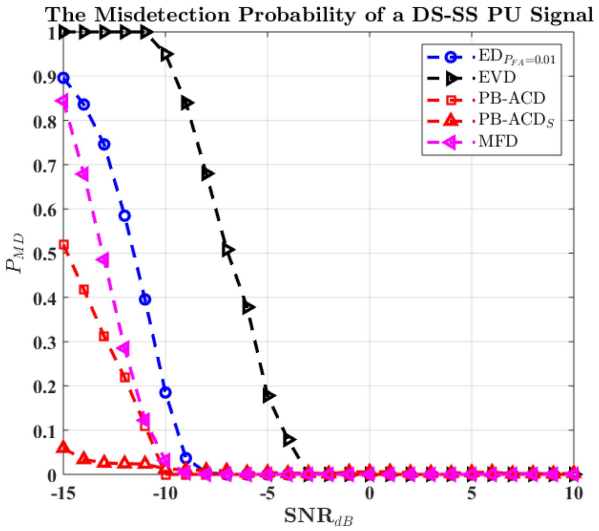

FIGURE 28. The misdetection probability of the PB-ACD as compared to the smoothed PB-ACD and different state-of-the-art techniques for detection a DS-SS signal for detection a DS-SS signal; PB-ACD_S denotes the smoothed PB-ACD technique.

Detection (MFD). The detection and misdetection probabilities are shown in Fig. 27 and Fig. 28, respectively. For the EVD technique, the detection performance is based on evaluating the maximum and the minimum eigenvalues of the covariance matrix of the received signal [45]. The inherited correlation between signal samples can be reflected in the eigenvalues of the covariance matrix which can be used to formulate the detection test statistic.

Deciding on the presence or absence of the PU signal depends on the ratio of the maximum to minimum eigenvalues. Even though the maximum-minimum EVD does not require any knowledge on the transmitted signal characteristics neither on the noise variance, its high computational complexity due to the high data processing is the main drawback. The desired expression of the detection threshold based on the probability of false alarm can be found in[4] [46]. For the MFD, its drawbacks are related to the perfect knowledge of the PU signal and the noise variance. In [47], the detection threshold of the suggested MFD is given as a function of SNR so at low SNR, the value of the detection threshold becomes higher such that the detection performance deteriorates.[5] In Fig. 27, the matched filter detector has the highest detection probability among the energy Detector and the eigenvalue-based detector at SNR of -15 dB, whereas the PB-ACD technique is higher in detection probability by 30% than the matched filter detector. However, as the SNR slightly increases to -12 dB, the PB-ACD and the MFD techniques perform similarly. By applying the smoothing process to the PB-ACD, the detection results increased by 40%. Moreover, Fig. 28 illustrates the efficacy of the PB-ACD technique to be less likely to miss-detect the presence of a DS-SS PU signal among the considered state-of-the-art techniques. For the IR-UWB signal, we used a Gaussian monocycle waveform to generate the transmitted pulses along with the passband BPSK modulation scheme. The impulse duration is 0.5 nsec, and the carrier frequency is 6 GHz.

The performance results are shown in Fig. 29 and Fig. 30. In Fig. 29, the PB-ACD outperforms the three considered state-of-the-art techniques over the SNR $[-15,-9]$ dB. At -8 dB, the PB-ACD and the Matched filter techniques have the same detection probability. Over about -8 dB, the Matched Filter Detector gives the highest detection

4. The approximated detection threshold of the EVD η_{EVD} is given by: $\eta_{EVD} = F_{app}^{-1}(1 - P_{FA})$; $F_{app}^{-1}(.)$ is the approximated distribution function of the eigenvalue ratio.

5. The detection threshold of the MFD, denoted by η_{MF}, is given by: $\eta_{MF} = Q^{-1}(P_{FA}\sqrt{E_s\sigma_w^2})$; E_s is the energy of the signal and σ_w^2 is the noise power.

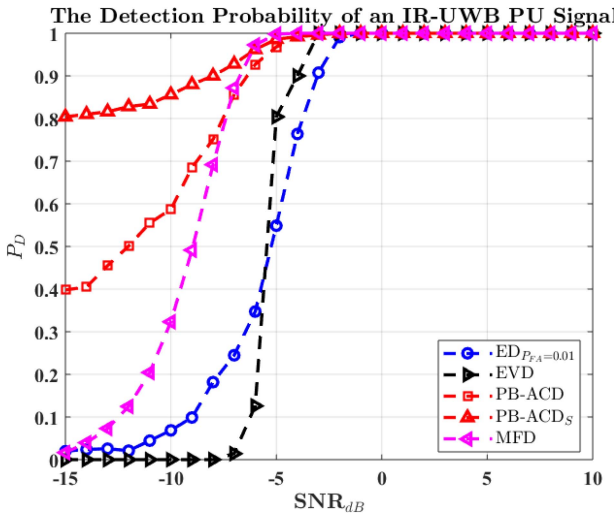

FIGURE 29. The detection probability of the PB-ACD as compared to the smoothed PB-ACD and different state-of-the-art techniques for detection an IR-UWB signal; $PB\text{-}ACD_S$ denotes the smoothed PB-ACD technique.

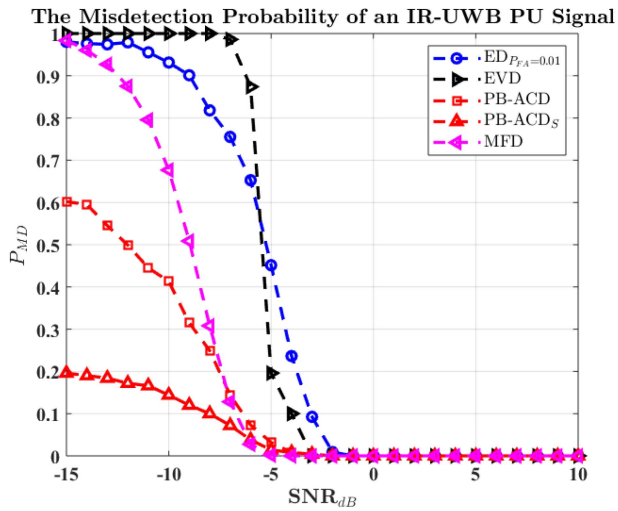

FIGURE 30. The misdetection probability of the PB-ACD as compared to the smoothed PB-ACD and different state-of-the-art techniques for detection an IR-UWB signal; $PB\text{-}ACD_S$ denotes the smoothed PB-ACD technique.

performance than the PB-ACD and the considered state-of-the-art techniques. To provide more improvement, we applied the smoothed PB-ACD. As shown in Fig. 30, the smoothed PB-ACD technique can detect the presence of the IR-UWB signal by approximately 40% detection probability as opposed to the PB-ACD technique. Also, it gives the lowest misdetection probability at low SNR values as opposed to the other considered detection techniques as shown in Fig. 30.

To sum up, as mentioned in Section III, we divide the WBSS problem into two phases, namely: the edge detection and PU detection phases. In the edge detection phase, the identification of the spectral boundaries is accomplished by the DLSD technique and the detection performance is compared to different wavelet-based spectrum sensing

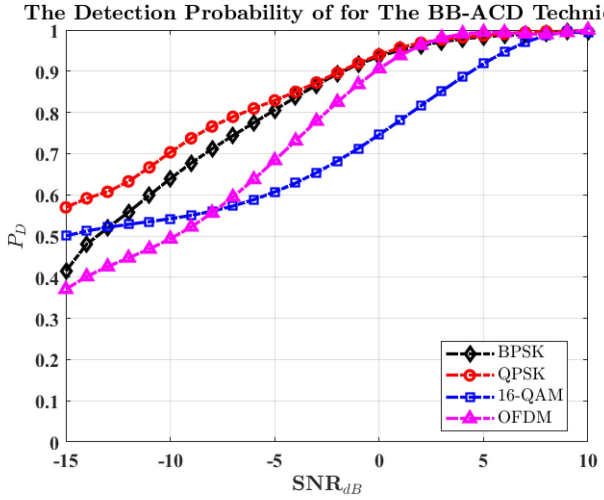

FIGURE 31. The detection probability of the BB-ACD technique for different modulation schemes.

techniques. In the PU detection phase, a suitable NBSS technique can be employed to analyze each subband in order to monitor its occupancy by a noise-like signal. To show the robustness of the PB-ACD and the improved PB-ACD techniques, we assumed an exact knowledge of the subband center frequencies and compared their detection performance for detecting noise-like signals to ED, MFD, and EVD techniques as shown in Fig. 27 to Fig. 30.

2) DETECTION OF NOISE-LIKE SIGNALS UNDER CARRIER FREQUENCY UNCERTAINTY BY THE BB-ACD TECHNIQUE:

In the single-band signal detection scenario, the operating frequency is usually known to the SU receiver. However, under multiband spectrum sensing scenario, and due to the edge-detection phase, the center frequencies of the subbands are unknown and may be subjected to frequency estimation errors. Thus, the BB-ACD technique is proposed to detect noise-like signals under carrier frequency uncertainty and its performance is compared with that of the PB-ACD technique. The simulations are averaged over 3000 Monte-Carlo realizations with the following parameters: the carrier frequency $f_c = 5$ GHz, and the employed sampling frequency f_s is 20 GHz. The performance of the proposed narrowband detector is measured in terms of the detection probability versus the SNR evaluated from -15 to 10 dB. To include the effect of carrier frequency uncertainty, we employed the example illustrated in Fig. 14 which results in a frequency shift of 0.4 GHz.

The applicability of the proposed BB-ACD technique for detecting different digital modulation schemes is tested for the case of the BPSK, QPSK, and 16-QAM modulation schemes as well as BPSK/OFDM PU signal as shown in Fig. 31. Further, we compare the BB-ACD technique with the PB-ACD when the operating carrier frequency is known to the CR receiver in Fig. 32. When the PB-ACD technique is applied under exact knowledge of the subband

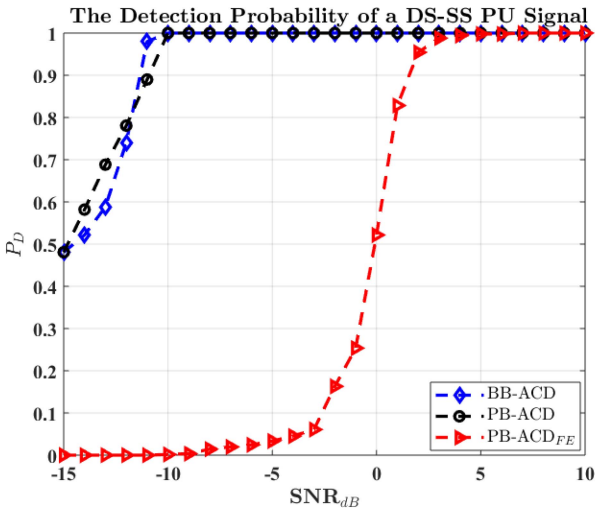

FIGURE 32. The detection probability of the BB-ACD as compared to the PB-ACD under carrier frequency uncertainty for detecting a DS-SS signal; PB-ACD$_{FE}$ refers to the applying the PB-ACD in case of frequency errors.

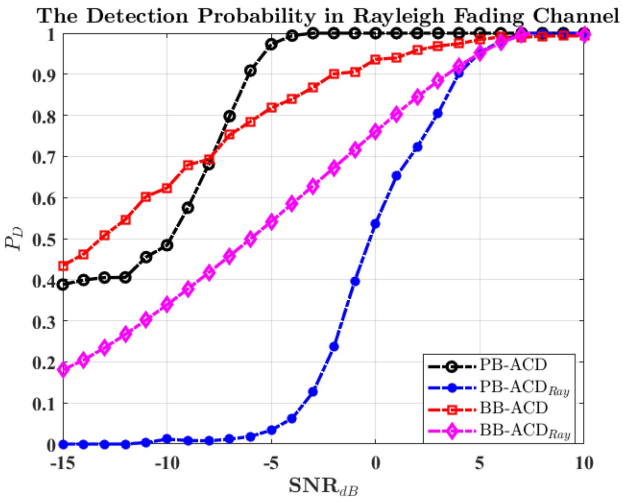

FIGURE 33. The detection performance of the BB-ACD technique as compared to the PB-ACD technique in a Rayleigh fading channel; PB-ACD$_{Ray}$ refers to employing the PB-ACD technique in Rayleigh fading channel.

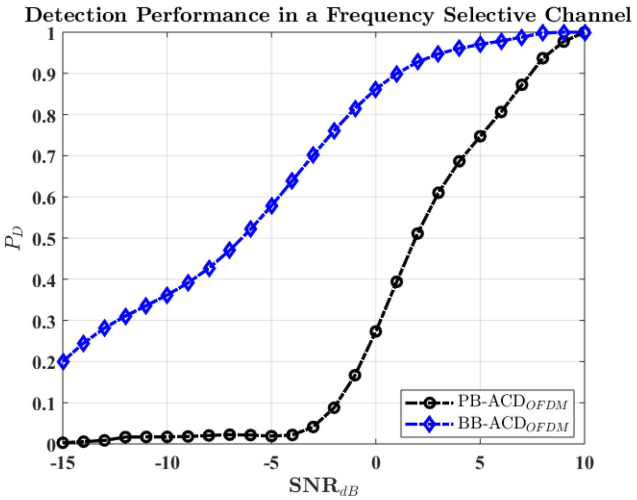

FIGURE 34. The detection performance of the BB-ACD technique as compared to the PB-ACD technique in a frequency selective fading channel.

center frequency, the achieved detection probability becomes approximately 50% higher than the same technique applied when there are errors in the center frequency values of the subbands of interest at SNR of -15 dB due to the detection dependency on the carrier frequency value. On the other hand, the proposed BB-ACD technique results in 50% detection probability at -15 dB and slowly increases to 100% at SNR of -6 dB. Precisely, the detection test statistic of the BB-ACD technique depends on averaging the periodic peaks that appeared in the power cepstrum of the baseband signal. At low SNR, these peaks have relatively low values as compared to the major peak that characterizes the test statistic of the PB-ACD technique. Thus, as the SNR increases, we notice a gradual increase in the detection performance of the BB-ACD technique.

Moreover, to test the robustness of the proposed BB-ACD technique in fading channels, we evaluate its detection performance as compared to the PB-ACD technique for detecting PU signals in a Rayleigh fading channel. Fig. 33 shows that the detection performance of the BB-ACD technique is superior to the PB-ACD for detecting a BPSK PU signal. Also, we notice a performance deterioration of the PB-ACD technique by around 40% when the PU signal experiences fading such that the detection probability drops to 0 at -15 dB. On the other hand, the detection probability of the BB-ACD technique drops to 20% at -15 dB when Rayleigh fading is encountered.

We also tested the performance of the proposed BB-ACD technique to detect an OFDM PU signal in frequency selective channel and compared the obtained results with the PB-ACD technique. The simulation of OFDM signals in AWGN or a frequency selective channel follows the IEEE 802.11 specifications [29]. The frequency selective channel is implemented as a 4-taps Finite Impulse Response (FIR) filter. The path delays vector is given as $\tau = [0, 100, 35, 120]$ μsec, and the average path gains vector is given by $P_G = [0, -1, -1, -3]$ dB. For a sample period $T_s = 1\mu$sec, the maximum Doppler frequency equals 100 kHz. The detection performance of the BB-ACD as compared to the PB-ACD under the Doppler frequency shift due to the frequency selective fading channel is shown in Fig. 34. According to our simulations, we find that the proposed BB-ACD technique gives better detection results than the PB-ACD technique at -15 dB, whereas the PB-ACD starts to significantly detect the PU presence above -4 dB. This means that the effect of the Doppler frequency shift deteriorates the PB-ACD performance, especially at low SNR values, while the BB-ACD technique can detect the OFDM PU signal successfully.

Another important performance metric to evaluate the efficacy of the proposed techniques is computational complexity. In this regard, we analyze the computational complexity

TABLE 6. Summary of the computational complexity of the DLSD algorithm as compared to the WTMP algorithm.

WTMP		DLSD	
Arithmetic Operations	**Complexity**	**Arithmetic Operations**	**Complexity**
Autocorrelation	$O(N_c^2)$	Autocorrelation	$O(N_c^2)$
FFT	$O(N_c \log N_c)$	FFT	$O(N_c \log N_c)$
Linear Convolution by a kernel of size K	$O(N_c K)$	Natural Logarithm using Arithmetic-Geometric Mean	$O(N_c \log N_c)$
Product of Modulus Maxima	$O(N_c)$	Automatic or numerical Differentiation	$O(N_c)$

of the DLSD edge detection algorithm followed by the BB-ACD technique and compare it with the WTMP edge detection technique followed by ED. For a 1D signal of size N_c, the edge detection algorithm given by the WTMP technique involves evaluating the autocorrelation of the received signal followed by the FFT operation to obtain the PSD. To identify the spectral boundaries, the received signal's PSD is filtered by the Fourier Transform of the smoothing wavelet function through a convolution operation. On the other hand, the proposed DLSD algorithm involves getting the autocorrelation, the PSD of the received signal followed by the gradient of the natural logarithm of the signal's PSD. Table 6 summarizes the complexity of the arithmetic operations involved in evaluating both algorithms.

To perform energy detection, the computational complexity requires $O(N_c)$ multiplications and $O(N_c - 1)$ for the averaging. For the BB-ACD technique, it requires $O(N_c K)$ for convolving the received signal with the Hilbert filter of size K, $O(N_c)$ for the SLD, and for the power cepstrum the complexity is similar to the DLSD algorithm except for that of the differentiation step. Based on Table 6, we find that the complexity of the WTMP is higher than the DLSD algorithm since the complexity of evaluating linear convolution is greater than that of the natural logarithm [48]. However, under the problem of frequency uncertainty, the BB-ACD has a higher complexity than ED or the BED despite its high detection accuracy. A trade-off analysis between the computational complexity and the maximum detection accuracy can be further investigated to highlight the competence of the proposed approach.

VI. CONCLUSION AND FUTURE WORK

In this paper, we proposed a wideband spectrum sensing approach based on cepstral analysis. It is shown that the spectral boundaries of the subbands comprising the target wide band can be well identified, in medium-to-high SNR environments (i.e., over the range [0, 6] dB), by employing the proposed DLSD algorithm. Although the detection of the spectral edges becomes difficult in low SNR environments (i.e., below 0 dB), the performance of the DLSD algorithm provides good detection results as compared to different wavelet-based approaches when further denoising is applied. For the PU detection phase, we tackled the problem of detecting noise-like signals in the SBSA and the MBSA scenarios. In the case of the SBSA, we proposed the improved PB-ACD technique to detect the presence of noise-like signals such as DS-SS and IR-UWB signals. The proposed detector outperformed different state-of-the-art techniques. Further, we addressed the problem of the carrier frequency uncertainty in the MBSA and presented the BB-ACD technique to provide better detection of possible noise-like signals in low SNR environments. The applicability of the proposed BB-ACD algorithm to different digitally modulated signals is evaluated. Also, the reliability of the BB-ACD technique is validated as opposed to the PB-ACD technique in frequency selective fading channels. As future work, the involvement of a reliable channel estimation process is essential to include its effect on the spectrum sensing results. Also, the trade-off between the computational complexity and the detection accuracy can be analyzed for the combined DLSD and BB-ACD techniques.

APPENDIX A

We need to get the constants a and b in order to verify that the chosen function $g(t)$ is a valid majorizer for $f(t)$, so based on the second condition of MM algorithm, we have:

$$g(t = t_k) = f(t = t_k) \tag{63}$$

accordingly, we get:

$$c = \frac{1}{T_c} - t_k\left(\frac{1}{T_c} - bt_k\right) \tag{64}$$

referring to the inequality in (37), we have:

$$bt^2 - \frac{t}{T_c} + \left(\frac{1}{T_c} - c\right) \; < \; 0 \tag{65}$$

then for $b > 0$:

$$4b\left(\frac{1}{T_c} - c\right) = \frac{1}{T_c^2} \tag{66}$$

substitute (65) in (67), for $u = bT_c t_k$ we have:

$$u^2 - u + \frac{1}{4} \geq 0 \tag{67}$$

thus, for a general expression:

$$b = \frac{1}{2T_c|t_k|}, \quad c = \frac{1 - 2|t_k|}{2T_c}. \tag{68}$$

APPENDIX B

Consider a random process $J = |\log[V]|$, and we seek the distribution of J if V follows $\chi^2_{(2)}$. Thus, J follows MLCS distribution. Based on the PDF approach, we find the required distribution by:

$$f_J(j) = \frac{f_V(v)}{|dJ/dV|}\Big|_{V=\pm J} \tag{69}$$

then, by substituting for $\frac{dJ}{dV} = \frac{V}{|V|}|$, we get:

$$f_J(j) = \frac{1}{2}\left[\exp\left(j - \frac{1}{2}\exp(j)\right) + \exp\left(-j - \frac{1}{2}\exp(-j)\right)\right]. \tag{70}$$

ACKNOWLEDGMENT

The authors gratefully acknowledge the contribution of M. E. S. Youssef from the Telecommunications and Signal Processing laboratory at McGill university, for the technical assistance provided in the analysis of the wavelet-based edge detection techniques.

REFERENCES

[1] M. J. Marcus, "Spectrum policy for radio spectrum access," *Proc. IEEE*, vol. 100, no. 2, pp. 1685–1691, May 2012.
[2] S. Sasipriya and R. Vigneshram, "An overview of cognitive radio in 5G wireless communications," in *Proc. IEEE Int. Conf. Comput. Intell. Comput. Res. (ICCIC)*, Chennai, India, Dec. 2016, pp. 1–5.
[3] T. S. Rappaport *et al.*, "Wireless communications and applications above 100 GHz: Opportunities and challenges for 6G and beyond," *IEEE Access*, vol. 7, pp. 78729–78757, 2019.
[4] E. Yaacoub and M.-S. Alouini, "A key 6G challenge and opportunity—Connecting the remaining 4 billions: A survey on rural connectivity," 2019. [Online]. Available: arXiv:1906.11541.
[5] A. Garhwal and P. P. Bhattacharya, "Dynamic spectrum access in cognitive radio: A brief review," *Int. J. Comput. Appl. Eng. Sci. Spec. Issue Comput. Netw. Security*, vol. 1, pp. 149–153, Dec. 2011.
[6] S. Mallat and W. L. Hwang, "Singularity detection and processing with wavelets," *IEEE Trans. Inf. Theory*, vol. 38, no. 2, pp. 617–643, Mar. 1992.
[7] E. Axell, G. Leus, E. G. Larsson, and H. V. Poor, "Spectrum sensing for cognitive radio : State-of-the-art and recent advances," *IEEE Signal Process. Mag.*, vol. 29, no. 3, pp. 101–116, May 2012.
[8] J. Jäntti, S. Chaudhari, and V. Koivunen, "Detection and classification of OFDM waveforms using cepstral analysis," *IEEE Trans. Signal Process.*, vol. 63, no. 16, pp. 4284–4299, Aug. 2015.
[9] B. P. Bogert, M. J. R. Healy, and J. W. Tukey, "The quefrency alanysis of time series for echoes; cepstrum, pseudo-autocovariance, cross-cepstrum and saphe cracking," in *Proceedings of Time Series Analysis*, M. Rosenblatt, Ed. New York, NY, USA: Wiley, 1963, ch. 15, pp. 209–243.
[10] T. Nguyen, B. L. Mark, and Y. Ephraim, "Spectrum sensing using a hidden bivariate markov model," *IEEE Trans. Wireless Commun.*, vol. 12, no. 9, pp. 4582–4591, Sep. 2013.
[11] Y. Sun, B. L. Mark, and Y. Ephraim, "Online parameter estimation for temporal spectrum sensing," *IEEE Trans. Wireless Commun.*, vol. 14, no. 8, pp. 4105–4114, Aug. 2015.
[12] A. Ghasemi and E. S. Sousa, "Spectrum sensing in cognitive radio networks: Requirements, challenges and design trade-offs," *IEEE Commun. Mag.*, vol. 46, no. 4, pp. 32–39, Apr. 2008.
[13] H. M. Farag and E. M. Mohamed, "Improved cognitive radio energy detection algorithm based upon noise uncertainty estimation," in *Proc. 31st Nat. Radio Sci. Conf. (NRSC)*, Cairo, Egypt, Apr. 2014, pp. 107–115.
[14] E.-N. S. E.-D. Youssef, "Advanced wavelet-based approach to spectrum sensing for cognitive radio networks," M.S. thesis, Dept. Electron. Commun. Eng., Arab Acad. Sci. Technol. Maritime Transp., Cairo, Egypt, 2013.
[15] A. Moawad, K.-C. Yao, A. Mansour, and R. Gautier, "Autocepstrum approach for spectrum sensing in cognitive radio," in *Proc. 15th Int. Symp. Wireless Commun. Syst. (ISWCS)*, Lisbon, Portugal, Aug. 2018, pp. 1–6.
[16] G. Burel, "Detection of spread spectrum transmissions using fluctuations of correlation estimators," in *Proc. IEEE Int. Symp. Intell. Signal Process. Commun. Syst. (ISPACS'2000)*, vol. 11. Honolulu, Hawaii, USA, 2000, p. B8.
[17] S. Rezk, C. Join, and S. El Asmi, "An algebraic derivative-based method for R wave detection," in *Proc. 19th Eur. Signal Process. Conf.*, Barcelona, Spain, Aug. 2011, pp. 1578–1582.
[18] Z. Tian and G. B. Giannakis, "A wavelet approach to wideband spectrum sensing for cognitive radios," in *Proc. 1st Int. Conf. Cognitive Radio Orient. Wireless Netw. Commun.*, Mykonos Island, Greece, Jun. 2006, pp. 1–5.
[19] Z. Xiaoli, "Edge detection algorithm based on multiscale product with Gaussian function," *Procedia Eng.*, vol. 15, pp. 2650–2654, Jan. 2011.
[20] S. E. El-Khamy, M. S. El-Mahallawy, and E.-N. S. Youssef, "Improved wideband spectrum sensing techniques using wavelet-based edge detection for cognitive radio," in *Proc. Int. Conf. Comput. Netw. Commun. (ICNC)*, San Diego, CA, USA, Jan. 2013, pp. 418–423.
[21] S. Jindal, D. Dass, and R. Gangopadhyay, "Wavelet based spectrum sensing in a multipath Rayleigh fading channel," in *Proc. 20th Nat. Conf. Commun. (NCC)*, Kanpur, India, Feb. 2014, pp. 1–6.
[22] A. Kumar, S. Saha, and R. Bhattacharya, "Wavelet transform based novel edge detection algorithms for wideband spectrum sensing in CRNs," *AEU Int. J. Electron. Commun.*, vol. 84, pp. 100–110, Feb. 2018.
[23] G. Hattab and M. Ibnkahla, "Multiband spectrum access: Great promises for future cognitive radio networks," *Proc. IEEE*, vol. 102, no. 3, pp. 282–306, Mar. 2014.
[24] D. G. Childers, D. P. Skinner, and R. C. Kemerait, "The cepstrum: A guide to processing," *Proc. IEEE*, vol. 65, no. 10, pp. 1428–1443, Oct. 1977.
[25] A. V. Oppenheim and R. W. Schafer, "From frequency to quefrency: A history of the cepstrum," *IEEE Signal Process. Mag.*, vol. 21, no. 5, pp. 95–106, Sep. 2004.
[26] E. Flinn, T. Cohen, and D. McCowan, "Detection and analysis of multiple seismic events," *Bull. Seismol. Soc. Amer.*, vol. 63, nos. 6–1, pp. 1921–1935, 1973.
[27] E. L. Ferguson, S. B. Williams, and C. T. Jin, "Improved multipath time delay estimation using cepstrum subtraction," in *Proc. IEEE Int. Conf. Acoust. Speech Signal Process. (ICASSP)*, Brighton, U.K., May 2019, pp. 551–555.
[28] G. Hua, J. Goh, and V. L. Thing, "Cepstral analysis for the application of echo-based audio watermark detection," *IEEE Trans. Inf. Forensics Security*, vol. 10, no. 9, pp. 1850–1861, Sep. 2015.
[29] F. Liedtke and U. Albers, "Evaluation of features for the automatic recognition of OFDM signals in monitoring or cognitive receivers," *J. Telecommun. Inf. Technol.*, vol. 84, no. 2, pp. 30–36, 2008.
[30] H. Cheng, B. L. Mark, and Y. Ephraim, "Wideband temporal spectrum sensing using cepstral features," in *Proc. IEEE 20th Int. Symp. World Wireless Mobile Multimedia Netw. (WoWMoM)*, Washington, DC, USA, Jun. 2019, pp. 1–6.
[31] J. M. Bruno and B. L. Mark, "A recursive algorithm for wideband temporal spectrum sensing," *IEEE Trans. Commun.*, vol. 66, no. 1, pp. 26–38, Jan. 2018.
[32] T. Scheuer and D. Wagner, "Deconvolution by autocepstral windowing," *Geophysics*, vol. 50, no. 10, pp. 1533–1540, 1985.
[33] E. Manasseh, S. Ohno, and M. Nakamoto, "Pilot symbol assisted channel estimation for OFDM-based cognitive radio systems," *EURASIP J. Adv. Signal Process.*, vol. 1, no. 1, p. 51, 2013.
[34] L. W. Couch, M. Kulkarni, and U. S. Acharya, *Digital and Analog Communication Systems*, vol. 6. Upper Saddle River, NJ, USA: Prentice Hall, 1997.
[35] S. M. Kay, "Fundamentals of statistical signal processing, vol. II: Detection theory," in *Signal Processing*. Upper Saddle River, NJ, USA: Prentice-Hall, 1998.
[36] J.-F. Bercher and C. Vignat, "On minimum fisher information distributions with restricted support and fixed variance," *Inf. Sci.*, vol. 179, no. 22, pp. 3832–3842, 2009.

[37] M. N. Kohan and H. Behnam, "Denoising medical images using calculus of variations," *J. Med. Signals Sens.*, vol. 1, no. 3, pp. 184–190, 2011.
[38] L. Chato, S. Latifi, and P. Kachroo, "Total variation denoising method to improve the detection process in IR images," in *Proc. IEEE 8th Annu. Ubiquitous Comput. Electron. Mobile Commun. Conf. (UEMCON)*, New York, NY, USA, Oct. 2017, pp. 441–447.
[39] I. Selesnick, *Total Variation Denoising (An MM Algorithm)*, NYU Polytechn. School Eng., New York, NY, USA, 2012.
[40] A. Chopra and H. Lian, "Total variation, adaptive total variation and nonconvex smoothly clipped absolute deviation penalty for denoising blocky images," *Pattern Recognit.*, vol. 43, no. 8, pp. 2609–2619, 2010.
[41] T. S. Rappaport *et al.*, *Wireless Communications: Principles and Practice*, vol. 2. Upper Saddle River, NJ, USA: Prentice-Hall PTR, 1996.
[42] S. Kay, "The effect of sampling rate on autocorrelation estimation," *IEEE Trans. Acoust., Speech, Signal Process.*, vol. 29, no. 4, pp. 859–867, Aug. 1981.
[43] K. Krishnamoorthy, *Handbook of Statistical Distributions With Applications*. Boca Raton, FL, USA: Chapman and Hall, 2006.
[44] S. C. Chapra, and R. P. Canale, *Numerical Methods for Engineers*. Boston, MA, USA: McGraw-Hill Higher Educ., 2010.
[45] P. Alvarez, N. Pratas, A. Rodrigues, N. R. Prasad, and R. Prasad, "Energy detection and eigenvalue based detection: An experimental study using gnu radio," in *Proc. 14th Int. Symp. Wireless Pers. Multimedia Commun. (WPMC)*, Brest, France, Oct. 2011, pp. 1–5.
[46] Y. Zeng and Y.-C. Liang, "Eigenvalue-based spectrum sensing algorithms for cognitive radio," *IEEE Trans. Commun.*, vol. 57, no. 6, pp. 1784–1793, Jun. 2009.
[47] F. Salahdine, H. El Ghazi, N. Kaabouch, and W. F. Fihri, "Matched filter detection with dynamic threshold for cognitive radio networks," in *Proc. Int. Conf. Wireless Netw. Mobile Commun. (WINCOM)*, Marrakech, Morocco, Oct. 2015, pp. 1–6.
[48] R. E. Blahut, *Fast Algorithms for Signal Processing*, 1st ed. Cambridge, U.K.: Cambridge Univ. Press, Jun. 2010.

AZZA MOAWAD (Member, IEEE) received the B.Sc. and M.Sc. degrees from the Electronics and Communications Department, Arab Academy for Science and Technology and Maritime Transport (AASTMT) in July 2007 and October 2012, respectively. She is currently pursuing the Ph.D. degree with the Laboratoire en Sciences et Techniques de l'Information, de la Communication et de la Connaissance, Bretagne Occidentale University. She has been working as an Assistance Lecturer with AASTMT since 2007. Her research interests are in the areas of signal processing, cognitive radio, and wireless communication.

KOFFI-CLÉMENT YAO (Member, IEEE) received the Ph.D. degree in optical signal processing and computer sciences from University Louis Pasteur, Strasbourg, in 1990. After his postdoctoral research period on optical neural networks with Ecole Nationale Supérieure des Téelécommunications (ENST), IMT Atlantique, Brest. He joined the French Naval Academy as an Assistant Professor in statistical signal processing in 1992. Since 2001, he has been an Assistant Professor with the Université de Bretagne Occidentale (University of Western Brittany), Brest, France. His research interest was focused on Pattern recognition in sonar imagery and blind signal separation in underwater acoustics channel. He is member of the laboratory Lab-STICC CNRS UMR 6285, Team Security, Intelligence and Integrity of Information (SI3). His present research interests concern wireless communications, blind interception of digital communication signals, and cognitive radio.

ALI MANSOUR (Senior Member, IEEE) received the M.S. degree in the electronic electric engineering from the Lebanese University, in September 1992, the M.Sc. and Ph.D. degrees in signal, image and speech processing from the Institut National Polytechnique de Grenoble-INPG. Grenoble, France, in July 1993 and January 1997, respectively, and the HDR degree (Habilitation a Diriger des Recherches) from the Universite de Bretagne Occidentale-UBO, Brest, France, in November 2006. From January 1997 to July 1997, he held a postdoctoral position with the Laboratoire de Traitement d'Images et Reconnaissance de Forme, INPG. From August 1997 to September 2001, he was a Researcher with the Bio-Mimetic Control Research Center, Institute of Physical and Chemical Research (RIKEN), Nagoya, Japan. From October 2001 to January 2008, he was holding a teacher-researcher position with the Ecole Nationale Supérieure des Ingénieurs des Etudes et Techniques d'Armement (ENSIETA), Brest. From February 2008 to August 2010, he was a Senior-Lecturer with the Department of Electrical and Computer Engineering, Curtin University of Technology, Perth, Australia. During January 2009, he held an invited professor position with the Universite du Littoral Cote d'Opale, Calais, France. From September 2010 to June 2012, he was a Professor with the University of Tabuk, Tabuk, Saudi Arabia. Since September 2012, he has been a Professor with the ENSTA-Bretagne, Brest. He has authored and coauthored three books. He is the first author of many papers published in international journals, such as the IEEE TRANSACTIONS ON SIGNAL PROCESSING, IEEE SIGNAL PROCESSING LETTERS, *NeuroComputing*, *IEICE*, and *Artificial Life and Robotics*. He is also the first author of many papers published in the proceedings of various international conferences. His research interests are in the areas of blind separation of sources, high-order statistics, signal processing, cognitive radio, robotics, and telecommunication. He was elected to the grade of IEEE Senior Member in February 2006. He has been a member of technical program committees in many international conferences. He was the chair, the co-chair, and a scientific committee member in various international conferences. He is an active reviewer for a variety of international journals in different engineering fields. He was a Lead Guest Editor of *EURASIP Journal on Advances in Signal Processing*—Special Issue on Signal Processing Methods for Diversity and Its Applications.

ROLAND GAUTIER (Member, IEEE) received the M.Sc. degree from the University of Nice, Sophia Antipolis, France, in 1995, where his research activities were concerned with the blind source separation of convolutive mixtures for MIMO systems in digital communications, the Ph.D. degree in electrical engineering from the University of Nice in 2000, where his research interests were in experiment design for nonlinear parameters models, and the Habilitation to Supervise Research (HDR) degree from the University of Brest in 2013 presenting an overview of his post-doctoral scientific research activities on the development of "Self-Configuring Multi-Standard Adaptive Receivers: Blind Analysis of Digital Transmissions for Military Communications and Cognitive Radio." From 2000 to 2001, he was an Assistant Professor with Polytech-Nantes, Engineering School, University of Nantes, France. Since September 2001, he has been worked with the University of Brest, France, as an Associate Professor in electronic engineering and signal processing. From 2007 to June 2012, he was Assistant Manager of the Signal Processing Team, Laboratory for Science and Technologies of Information, Communication and Knowledge (Lab-STICC-UMR CNRS 6285). Since July 2012, he is the Manager of the Defense Research Axis, COM Team, Lab-STICC. His general interests lie in the area of signal processing and digital communications. His current research focuses on digital communication intelligence, analysis, and blind parameters recognition, multiple-access and spread spectrum transmissions, cognitive and software radio, cybersecurity, physical layer security for communications, drones communications detection, and jamming. Since 2018, he is the holder of the "CyberIoT" Chair of Excellence.